*in silico Plants*, 2023, **5**, 1–17
https://doi.org/10.1093/insilicoplants/diad014
Advance access publication 6 October 2023
**Original Research**



# Original Research

# Optimal coordination between photosynthetic acclimation strategy and canopy architecture in two contrasting cucumber cultivars

Yi-Chen Pao,[1,*,3] Hartmut Stützel,[1] and Tsu-Wei Chen[2,*]

[1]Institute of Horticultural Production Systems, Leibniz Universität Hannover, Lower Saxony, Herrenhäuser Straße 2, 30419 Hannover, Germany.
[2]Albrecht Daniel Thaer-Institute of Agricultural and Horticultural Sciences, Humboldt-Universität zu Berlin, Lentzeallee 75, 14195 Berlin, Germany.

[*]Corresponding authors' e-mail addresses: tsu-wei.chen@hu-berlin.de; yi-chen.pao@thuenen.de
[3]Present address: Institute of Rural Studies, Johann Heinrich von Thünen-Institute, Federal Research Institute for Rural Areas, Forestry and Fisheries, Braunschweig, Germany.

Guest Editor: Junqi Zhu

Editor-in-Chief: Stephen P Long

## ABSTRACT

Crop varieties differing in architectural characteristics (AC) vary in their intra-canopy light distribution. To optimize canopy photosynthesis, we hypothesize that varieties with contrasting AC possess different photosynthetic acclimation strategy (PAS) with respect to photosynthetic nitrogen ($N_p$) partitioning. We firstly used *in silico* experiments to test this hypothesis and suggested a trade-off in $N_p$ partitioning between carboxylation and light harvesting to achieve optimal coordination between PAS, AC and growing light environment. Then, two cucumber (*Cucumis sativus* L.) cultivars, Aramon and SC-50, which were bred under greenhouse vertical single-stem and field creeping multi-branch canopy, were selected for studying their differences in AC and PAS using greenhouse and growth chamber experiments, respectively. In the greenhouse, more horizontal leaves of SC-50 resulted in steeper intra-canopy light gradient and a higher degree of self-shading, especially in the upper canopy layer. In growth chamber experiments, Aramon invested more leaf nitrogen into photosynthesis than SC-50, and the proportion ($p_{Np}$) increased as light was reduced. In contrast, $p_{Np}$ of SC-50 did not respond to light but SC-50 partitioned its limited $N_p$ between carboxylation and light harvesting functions more effectively, showing a strategy particularly advantageous for canopies with a high degree of self-shading. This is further confirmed by additional *in silico* experiments showing that $N_p$ partitioning of SC-50 coped better with the impact of strong light competition caused by low light and by leaf clumping under high planting density. These findings provide a comprehensive perspective of genotypic variation in PAS, canopy architectures and their optimal coordination.

**KEYWORDS:** Canopy structure; functional-structural plant model; intra-canopy light distribution; light competition; light extinction coefficient; multi-layer model; nitrogen partitioning; photosynthetic protein turnover; plant architecture; varietal variation.

## 1. INTRODUCTION

Architectural characteristics (AC), from phyllotaxis to leaf morphology, determine intra-plant light attenuation (Brites and Valladares 2005; Chen *et al.* 2014b; Zhang *et al.* 2014; Tang *et al.* 2019) and self-shading (Falster and Westoby 2003), and explain most of the variation in light capture across species (Falster and Westoby 2003; Duursma *et al.* 2012). The degree of inter-plant competitiveness for light is likely to indirectly drive the selection for yield during the breeding process (Chen *et al.* 2019; Perez *et al.* 2019). Light attenuation through homogeneous canopies can be described by the Beer–Lambert law, which depends on leaf area index (LAI) and light extinction coefficient ($k$, de Pury and Farquhar 1997; Monsi and Saeki 2005). The latter can be considered as a function of canopy clumpiness and leaf angle distribution (Monsi and Saeki 2005; Chen *et al.* 2008; Zhang *et al.* 2014). Assuming a vertical sun direction, a more vertical angle distribution leads to a lower $k$ (Hikosaka and Hirose 1997; Zhang *et al.* 2014) and a more homogeneous vertical light distribution in canopies by improving light transmission (Falster and Westoby 2003; Truong *et al.* 2015). In contrast, a canopy

with more horizontally oriented leaves intercepts more light per unit leaf area, which is described by a higher $k$ (Zhu *et al.* 2010; Chen *et al.* 2014b) and a higher degree of self-shading. As a result of natural or artificial selection, plants developed specific spatiotemporal display of their leaf surfaces targeted to achieve balances in aspects of energy exchange (Niinemets *et al.* 2007; Niklas 2013), energy cost (Okabe 2015) and biophysical constraints (Pearcy *et al.* 2004) to thrive under their specific environmental conditions and with their cohabitants (Whitman and Aarssen 2010).

Natural variation in AC is subjected to genetic controls and their effects on phenotypic plasticity to the growing environments (e.g. Truong *et al.* 2015; Mantilla-Perez and Salas Fernandez 2017; Alqudah *et al.* 2018). Plant architecture is an essential component of fitness under inter- and intra-genotypic light competition (Hikosaka and Hirose 1997; Song *et al.* 2013). Selection pressure in terms of light competition explains why some AC observed in nature (branch angle distribution, Honda and Fisher 1978; coordination between architectural traits, Brites and Valladares 2005; leaf size and amount, Whitman and Aarssen 2010; leaf phyllotaxis, Strauss *et al.* 2020) as well as in major crops (Flood *et al.* 2011) appear optimized for canopy light interception. Theoretically, a strategy striving for maximal biomass production at the individual level should combine maximal light energy capture for photosynthesis and maximal efficiency of photosynthesis to convert energy into photo-assimilates (Evans 2013).

Architectural ideotypes (Song *et al.* 2013; Chen *et al.* 2014b, 2015; Perez *et al.* 2018; Chang *et al.* 2019; Tang *et al.* 2019) and cultural practices (planting pattern and density; Maddonni *et al.* 2001b; Drouet and Kiniry 2008) that maximize light interception are of great interest for breeding programs and crop management (Perez *et al.* 2019). However, light transmission within canopies is temporally dynamic due to continuous alteration of AC and thus $k$ with canopy development (Campbell and Norman 1989; Tahiri *et al.* 2006; Chen *et al.* 2014b), making coordination of resource use with local light availability crucial for efficient generation of photo-assimilates (Niinemets *et al.* 2015; Chang *et al.* 2019; Poorter *et al.* 2019).

Photosynthesis is the light-driven conversion of $CO_2$ into biomass through a cascade of biochemical processes, namely light harvesting, conversion of light energy into chemical energy, and carboxylation catalysed by the enzyme Rubisco (Farquhar *et al.* 1980). The capacities of these functions depend on the amount of nitrogen invested in the corresponding proteins (Evans and Seemann 1989; Hikosaka and Terashima 1996; Evans and Clarke 2019). The balance between light capture and conversion of photo-assimilates is essential as it regulates photosynthetic nitrogen use efficiency (PNUE; Evans 1989; Ishimaru *et al.* 2001; Hikosaka, 2010; Zhu *et al.* 2010; Song *et al.* 2017). Improvement in PNUE is desirable since nitrogen is one of the most limiting resources for plant growth (Evans 1989; Hikosaka and Terashima 1996; Aerts and Chapin 1999; Hikosaka 2010; Evans and Clarke 2019).

Driven by the need to use nitrogen efficiently, plants have mechanisms of light acclimation (Werger and Hirose 1991; Anten *et al.* 1995; Trouwborst *et al.* 2010; Osada *et al.* 2014; Hikosaka, 2016). At canopy level, between-leaf distribution of photosynthetic nitrogen ($N_p$) was reported to correlate with intra-canopy light distribution across species (Hikosaka *et al.* 2016), implying a generic light-dependent strategy for distributing $N_p$. At leaf level, an increase in PNUE can be achieved by shifting $N_p$ partitioning towards limiting photosynthetic functions according to light availability (Terashima and Evans 1988; Evans 1989; Hikosaka and Terashima 1996; Evans and Poorter 2001; Trouwborst *et al.* 2011; Song *et al.* 2017; Yin *et al.* 2019). This was supported by modelling studies (Evans 1993b; Pons and Anten 2004; Pao *et al.* 2019a) indicating higher sensitivity of plant carbon assimilation to $N_p$ partitioning between photosynthetic functions (carboxylation, $N_V$, electron transport, $N_J$, and light harvesting, $N_C$) than to nitrogen distribution between leaves. Recent approaches have applied the concept of protein turnover for the three functional pools of photosynthetic proteins to explore environmental impacts on the dynamics of $N_p$ partitioning (Muller and Martre 2019; Pao *et al.* 2019a, b). Using this model, photosynthetic acclimation strategy (PAS) of $N_p$ partitioning of a greenhouse cucumber cultivar was predicted to be optimal in combination with its AC for maximizing carbon assimilation (Pao *et al.* 2019a).

Since variation in AC among crop varieties results in different light distribution within their canopies, we first hypothesize an optimal coordination between AC and PAS to maximize canopy photosynthesis. To test this hypothesis, we first used *in silico* experiments to derive a generalized pattern of optimal coordination between PAS, AC and light intensity in a virtual cucumber variety. Based on this hypothesis, different PAS could be expected in real-world cucumber varieties bred under contrasting canopy architectures and environments. To demonstrate this, we selected two cultivars, one was bred under greenhouse conditions with vertical single-stem training while the other in the field with a creeping multi-branch canopy, and quantified their variations in AC, intra-canopy light distribution and PAS using a series of greenhouse and growth chamber experiments. We further hypothesized that variety-specific PAS is co-selected with AC during yield-driven breeding process that optimizes canopy photosynthesis by coordination between PAS and AC. This hypothesis was tested using another series of *in silico* experiments. Combining real-world and *in silico* experiments, we provide a comprehensive perspective of genotypic variation in PAS canopy architectures and their optimal coordination.

## 2. MATERIALS AND METHODS

### 2.1 Definition of PAS

PAS is determined by the turnover of photosynthetic proteins and partitioning of photosynthetic nitrogen ($N_p$ per leaf area; mmol N $m^{-2}$). This can be well-described by a photosynthetic protein turnover model (Pao *et al.* 2019a, b), and the model parameters can be used to define PAS. Here, $N_p$ is simplified as the sum of nitrogen in the proteins involved in carboxylation, $N_V$, electron transport, $N_J$, and light harvesting, $N_C$ (Buckley *et al.* 2013). The photosynthetic nitrogen pool $N_V$ includes only Rubisco and represents the nitrogen contributing to carboxylation capacity. Pool $N_J$ includes electron transport chain, photosystem II core and Calvin cycle enzymes other than Rubisco. $N_C$ includes photosystem I core and light harvesting complexes I and II (Buckley *et al.* 2013). The rate of $N_X$ change at a given leaf age $t$ (°Cd) is determined by the instantaneous protein synthesis

$S_X$ (mmol N m$^{-2}$ °Cd$^{-1}$) and degradation $D_X$ (mmol N m$^{-2}$ °Cd$^{-1}$) rates of the corresponding enzymes and protein complexes:

$$dN_X/dt = S_X - D_X \quad (1)$$

Protein degradation rate $D_X$ is governed by first-order kinetics (Verkroost and Wassen 2005; Li *et al.* 2017; see Supporting Information—Eqn S1), while protein synthesis is described by an age-dependent logistic function [see Supporting Information—Eqn S2] with a potential rate of $S_{pot,X}$ (mmol N m$^{-2}$ °Cd$^{-1}$), where light acclimation comes into play:

$$S_{pot,X} = S_{mm,X} \times k_{I,X} \times I_d / (S_{mm,X} + k_{I,X} \times I_d) \times r_{N,X} \quad (2)$$

For a pool $X$, $S_{mm,X}$ (mmol N m$^{-2}$ °Cd$^{-1}$) describes its maximal protein synthesis rate, and rate constant $k_{I,X}$ controls how $S_{pot,X}$ increases with daily incident photon integral $I_d$ (mol photon m$^{-2}$ d$^{-1}$). The factor $r_{N,X}$ denotes the normalized effect of nitrogen limitation in protein synthesis [see Supporting Information—Eqn S3]. In this paper, PAS is represented by the pool-specific responses of $S_{pot,X}$ to light, which results in the acclimation of $N_p$ and its partitioning between functions. Preference of $N_p$ partitioning to a given function $X$ was described by its relative potential synthesis rate (rel$S_{pot,X}$), the ratio between $S_{pot,X}$ and the sum of $S_{pot}$ of all three pools.

One of the objectives of this study is to identify PAS that maximizes daily carbon assimilation (DCA, mol $CO_2$ d$^{-1}$ per plant) through optimal potential protein synthesis rate ($S_{pot,op,X}$), while keeping $N_{plant}$ and $N_{leaf}$ unmodified for a given architecture (Pao *et al.* 2019a, *in silico* Experiments 1 and 3, see the Sections 2.2 and 2.9 below). The optimization process maximized DCA of our model (see the Section 2.2 below) was carried out using package '*DEoptim*' in R (R Core Team 2019). To find the optimum, PAS was modified by introducing a factor $f_{p,X}$, ranging from 0.2 to 2.0, into Eqn 2 to manipulate the potential protein synthesis rate $S_{mm,X}$ of the functional nitrogen pool $X$ (Pao *et al.* 2020):

$$S_{pot,op,X} = S_{mm,X} \times f_{p,X} \times k_{I,X} \times I_d / (S_{mm,X} \times f_{p,X} + k_{I,X} \times I_d) \times r_{N,X} \quad (3)$$

High $f_{p,X}$ leads to high synthesis rates and partitioning to pool $X$. Architectures digitized in the fourth week were used in the simulation under various planting densities. The relative change in DCA resulting from optimal PAS ($DCA_{op}$) was calculated in comparison to the DCA under control scenario ($DCA_{ck}$), where $f_{p,X}$ equals one. An index of optimality (%) was then calculated as:

$$\text{Optimality} = \left(1 - \frac{DCA_{op} - DCA_{ck}}{|DCA_{op}|}\right) \times 100 \quad (4)$$

### 2.2 In silico Experiment 1—Testing the optimal coordination between functional photosynthetic acclimation strategy and canopy AC

To explore the optimal coordination between PAS and AC that maximizes daily carbon assimilation (DCA, sum of leaf photosynthesis, mol $CO_2$ d$^{-1}$ per plant) of the whole canopy, we conducted *in silico* experiments using a well-validated one-dimensional multi-layer model of greenhouse cucumber (Pao *et al.* 2021), coded in R (R Core Team 2019). The complete model is described in Supporting Information—Method S1. In short, the model described the development of new leaves (new layers) using the concept of phyllochron. We used greenhouse 3D-architecture as input (Pao *et al.* 2021, see also Supporting Information—Method S1) to derive the 'correct' light extinction coefficient to calculate light interception in each canopy layer using Beer–Lambert law (see Supporting Information—Eqn S14; Monsi and Saeki 2005; Pao *et al.* 2021). Photosynthetic nitrogen per unit leaf area $N_p$ (mmol N m$^{-2}$) was simulated, with a time step of 0.1 °Cd and environmental input of daily incident photosynthetic photon integrals (DPI), nitrogen supply level and mean air temperature (mean = 23.4 °C, similar to greenhouse conditions). Diurnal changes of photosynthetic photon intensity above the canopy were simulated using DPI, 0.1-h time step and 14.4-h day length by a cosine bell function (Kimball and Bellamy 1986). Leaf photosynthesis was calculated under conditions of leaf-to-air vapor pressure deficit ($D$) of 1.2 kPa and ambient $CO_2$ concentration of 400 μmol $CO_2$ mol$^{-1}$. Model variables and coefficients are listed in Supporting Information—Tables S1 and S2.

Since multiple parameters in the model are involved in AC and this hinders the algorithms for searching optimum, further simplification of AC is required. In this *in silico* experiment, canopy architecture was represented by a virtual cucumber variety with all leaves having a given absolute angle $\beta_{abs}$ relative to horizontal (°) in the canopy, with an LAI and leaf area distribution between layers of an intermediate type between cultivars Aramon and SC-50 (see the Section 2.3). Then, the package '*DEoptim*' in *R* (R Core Team 2019) was used to find the optimal $f_{p,X}$ (Eqn 3) that maximize DCA for $\beta_{abs}$ ranging between 15° and 75°. The optimization kept nitrogen content per leaf and per plant unmodified (Pao *et al.* 2019a). As $\beta_{abs}$ varied, light extinction coefficient ($k$) also changed accordingly:

$$k = \frac{0.95 - 0.32}{1 + \exp\left(\frac{54.4 - \beta_{abs}}{-17.9}\right)} + 0.32 \quad (5)$$

where increasing $\beta_{abs}$ led to decreasing $k$, ranging between 0.4 and 0.9 (derived from Fig. 7 in Monsi and Saeki 2005). For a given $\beta_{abs}$, $k$ is assumed unchanged over the day for simplification. Altogether, *in silico* experiments used a multi-layer model with a uniform leaf extinction coefficient for each layer (one leaf per layer, since cucumber plants were vertically trained using single-stem system, Fig. 1A) and the radiation intensity and photosynthetic rate for each leaf were calculated under the assumption that spacial heterogeneity of photosynthetic capacity within a leaf is negligible.

After maximizing DCA, optimal potential synthesis rates under daily incident light levels at the leaf (ranging between 2 and 20 mol m$^{-2}$ d$^{-1}$) was obtained. To visualize the coordination between PAS and AC, The optimal relative potential synthesis rate (rel$S_{pot,op,X}$) was then calculated as $S_{pot,X}$ divided by the sum of $S_{pot,op}$ of all three functions to indicate the relative preference in $N_p$ investment under given $\beta_{abs}$ and light conditions.

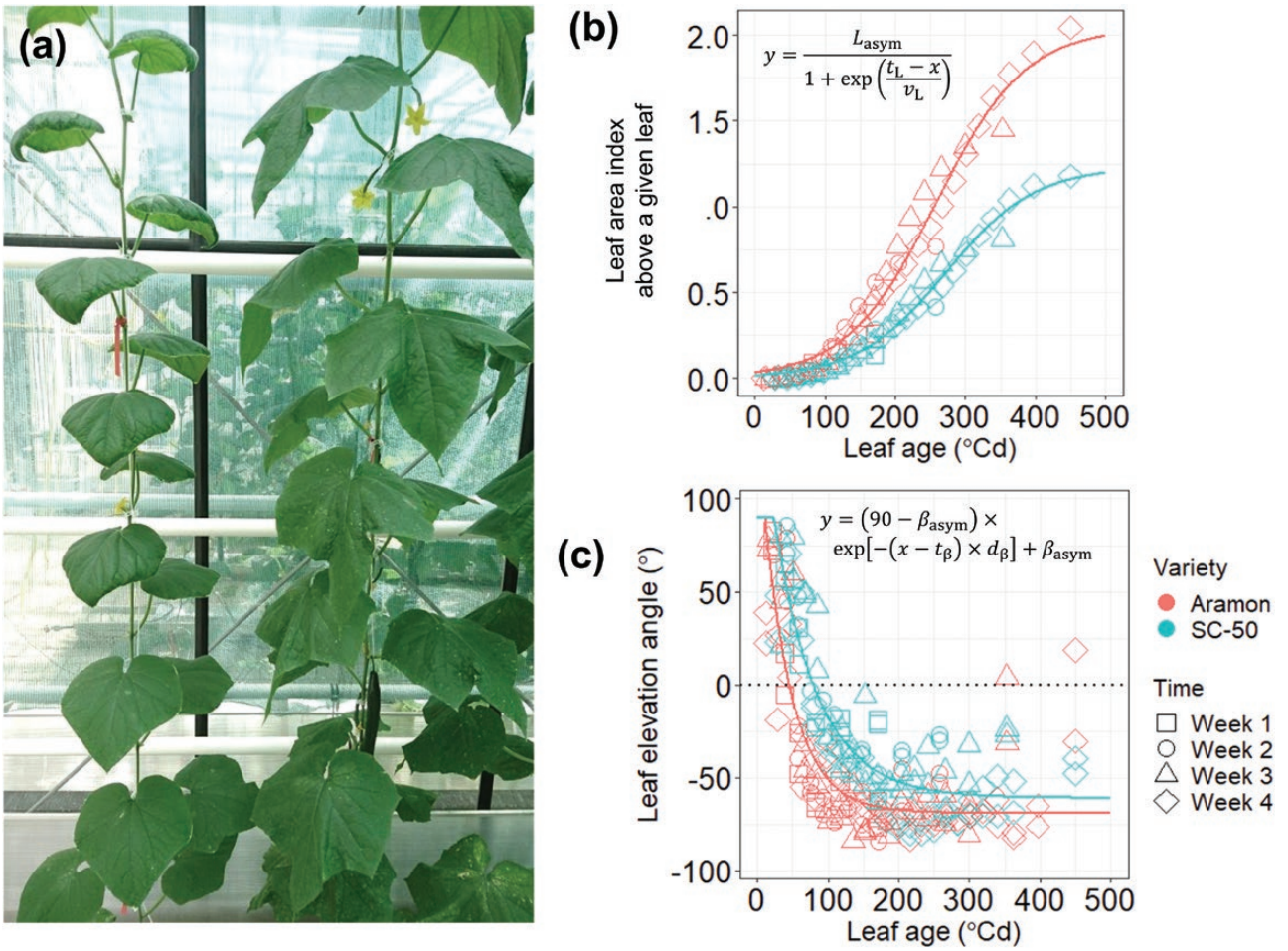


**Figure 1.** (A) Differences in plant morphology in two cucumber (*Cucumis sativus* L.) cultivars, SC-50 (left) and Aramon (right). Both are grown under single-stem training system in the greenhouse. (B) LAI at a given leaf ($L$) is accumulated from top to a given leaf at a plant density of 1.33 plants $m^{-2}$, fitted (lines) to Eqn 5. (C) Leaf elevation angle (°) measured in four consecutive weeks (indicated by different symbols) using digitization, fitted (lines) to Eqn 6. Elevation angles of 90° and −90° denote vertical leaves pointing up- and downwards, respectively, and 0° indicates a horizontal plane (dotted line).

### 2.3 Plant materials

To demonstrate that optimal coordination between PAS and AC could be co-selected during yield-driven breeding process, two high-performance cucumber (*Cucumis sativus* L.) cultivars, Aramon (Rijk Zwaan, De Lier, the Netherlands) and SC-50 (PI 234517, US National Plant Germplasm System; Barnes and Epps 1956), were selected and cultivated in the Institute of Horticultural Production Systems, Leibniz Universität Hannover, Germany (52° 39′ N, 9° 70′ E). Aramon is an F1 hybrid cultivar especially suitable for greenhouse production due to its stable gynoecy (Zhang *et al.* 2021) and parthenocarpy. SC-50 is a monoecious and open-pollinated cultivar bred by backcrossing an Indian landrace (PI 197087, US National Plant Germplasm System) with the recurrent parent, cultivar Ashley (AMES 4833, US National Plant Germplasm System), an heirloom variety adapted to the field conditions in South Carolina, USA. The variations in the plant architecture can be visually observed (Fig. 1A).

### 2.4 Quantifying the dynamics of AC using greenhouse experiment

To quantify the differences of AC between the two selected varieties, greenhouse experiment was carried out from 4 April to 3 May 2017 to assess plant AC. Sowing, seedling nursery and plant care were described in detail by Pao *et al.* (2020). In short, plants with three true leaves (plant height ca. 20 cm) were transferred onto rock-wool slabs in a greenhouse with a plant density of 1.33 plants $m^{-2}$ (1.5 m row distance and 0.5 m plant distance) and trained vertically in a single-stem system with all side shoots constantly removed (Fig. 1A). Plants of both cultivars were spaced and trained following the same practice and supplied with a nutrient solution containing 10 mM $NO_3^-$ by drip irrigation. Average daily photosynthetic photon integrals (DPI) above the canopy was 21.33 mol photon $m^{-2}$ $d^{-1}$ during the experimental period with an average day length of 14.4 h. Air temperature (min. 21.5 °C, max. 25.5 °C, average 23.4 °C) was recorded continuously using data loggers positioned in the middle of the canopy. Plant AC were obtained using a 3D digitizer (Fastrak; Polhemus, Colchester, USA) according to Chen *et al.* (2014a) on two representative plants of each variety, in four consecutive weeks on the 8th, 15th, 22nd and 29th days after transplanting.

To compare the dynamic change of AC between genotypes, snapshots of cumulative LAI at individual leaves $L$, calculated based on the destructive measurements, and their elevation

angles $\beta$ (°), measured by the 3D digitizer, were related by the thermal ages $t$ (°Cd, with base temperature of 10 °C for cucumber; Savvides *et al.* 2016) of the respective leaves. LAI above a given leaf increases logistically with its $t$ from zero to an asymptote $L_{asym}$, with an inflection point occurring at $t_L$ (°Cd), and the shape of the curve is determined by $\nu_L$:

$$L = L_{\text{asym}} / \{1 + \exp[(t_L - t)/\nu_L]\} \quad (6)$$

The elevation angle $\beta$ is defined as the angle between the line connecting the base to the tip of a lamina, and the horizontal plane. Elevation angles of 90° and −90° denote vertically upwards and downwards oriented leaves, respectively, while 0° indicates horizontal orientation. Newly appearing leaves have a $\beta$ of maximum 90°, followed by a decrease starting at a leaf age of $t_\beta$ (°Cd) by a constant $d_\beta$ (°Cd$^{-1}$) to an asymptote of $\beta_{asym}$ (°):

$$\beta = (90 - \beta_{\text{asym}}) \times \exp[-(t - t_\beta) \times d_\beta] + \beta_{\text{asym}} \quad (7)$$

Mathematically, $\beta$ is larger than 90° when $t$ is smaller than $t_\beta$. In this case, $\beta$ is set to a maximum of 90°.

### 2.5 Determining light extinction coefficient using static virtual 3D canopies

All *in silico* experiments of this study assumed one-dimensional light model using Beer–Lamber´s law, where homogeneous canopy is assumed. The potential biases from this assumption can be rectified if light extinction coefficient, $k$, can be correctly estimated from an accurately simulated 3D canopy (Pao *et al.* 2021). Therefore, virtual canopies were reconstructed in software GroIMP (Kniemeyer 2008) using digitized data (Chen *et al.* 2014a, 2018). Reconstructions were coupled with a light model to simulate light transmission through canopies for determining $k$ [see Supporting Information—Methods S1]. The values of $k$ at various canopy stages was determined and described by a function of cumulative LAI $L$, where $k$ increased to a maximum of $k_{max}$ when $L$ reached $L_k$ and then decreased to a minimum $k_{min}$, where $\nu_k$ determines the curve shape:

$$k = (k_{\max} - k_{\min}) \times \exp\left\{-0.5 \times \left[\frac{\ln\left(\frac{L}{L_k}\right)}{\nu_k}\right]^2\right\} + k_{\min} \quad (8)$$

### 2.6 Growth chamber experiment to quantify photosynthetic acclimation

The experiment was conducted with factorial combinations of three light and three nitrogen supply levels to parameterize the dynamics of photosynthetic protein turnover. Sowing, seedling nursery and treatment were described in detail by Pao *et al.* (2020). In brief, cucumber plants with two true leaves (plant height ca. 10 cm) were transferred to a hydroponic system with three nitrogen levels, 9.6, 4.6 and 2.3 mM $NO_3^-$, in combination with three constant light conditions (average PPFD incident on sampled leaves were 669, 329 and 102 µmol photon m$^{-2}$ s$^{-1}$ with a 12-h photoperiod). Sampled laminae were kept horizontally for full exposure to incoming light (for details see Pao *et al.* 2020). Air temperature around the leaves was recorded continuously using data loggers (Tinytag; Gemini Data Loggers, Chichester, UK).

Gas exchange was measured every 3 days at 12-time points, where the age of measured leaves ranged from 45 °Cd to 558 °Cd. Using a portable photosynthesis system (LI-6400XT; LI-COR, Lincoln, NE, USA), light-saturated net photosynthesis rate under photosynthetic photon flux density (PPFD) of 1300 µmol photon m$^{-2}$ s$^{-1}$ ($A_{1300}$, µmol $CO_2$ m$^{-2}$ s$^{-1}$) was measured and light response curves were determined. All measurements were carried out under sample $CO_2$ concentration of 400 µmol mol$^{-1}$ and leaf temperature 25 °C (details see Pao *et al.* 2020). Daytime respiration rate $R_d$ (µmol $CO_2$ m$^{-2}$ s$^{-1}$), maximal carboxylation rate ($V_{cmax}$, µmol $CO_2$ m$^{-2}$ s$^{-1}$), maximal electron transport ($J_{max}$, µmol e$^-$ m$^{-2}$ s$^{-1}$) and mesophyll conductance $g_m$ (mol $CO_2$ m$^{-2}$ s$^{-1}$) were estimated according to the protocol of Pao *et al.* (2020). Immediately after gas exchange measurements, leaves were harvested to determine leaf area, and then freeze-dried and ground into fine homogenized powder for total nitrogen ($N_t$, mmol m$^{-2}$; Nelson and Sommers 1980), nitrate-nitrogen ($N_n$, mmol m$^{-2}$; Cataldo *et al.* 1975) and leaf chlorophyll (*Chl*, mmol m$^{-2}$; Lichtenthaler 1987) analyses. The leaf powder required for the analyses were 100–150 mg, 100–200 mg and 5 mg, respectively. In total, 648 samples/curves were analysed. Photosynthetic nitrogen pools, $N_V$, $N_J$ and $N_C$, were estimated from $V_{cmax}$, $J_{max}$ and *Chl*, respectively (Buckley *et al.* 2013):

$$N_V = V_{cmax}/\chi_V \quad (9a)$$

$$N_J = J_{max}/\chi_J \quad (9b)$$

$$N_C = \frac{Chl - N_J \times \chi_{CJ}}{\chi_C} \quad (9c)$$

where $\chi_V$ (µmol $CO_2$ mmol$^{-1}$ N s$^{-1}$) is carboxylation capacity per unit Rubisco nitrogen, and $\chi_J$ (µmol e$^-$ mmol$^{-1}$ N s$^{-1}$) is the electron transport capacity per unit electron transport nitrogen. $\chi_{CJ}$ (mmol mmol$^{-1}$ N) and $\chi_C$ (mmol mmol$^{-1}$ N) are conversion coefficients for chlorophyll per electron transport nitrogen and per light harvesting component nitrogen, respectively. The $N_p$ partitioning fraction of a pool $X$, $p_X$, is the ratio of nitrogen in a pool $X$, $N_X$ (mmol N m$^{-2}$), to $N_p$. The fraction $p_{Nf}$ of organic nitrogen in structure and other functioning other than photosynthesis in $N_t$ was calculated as $[(N_t - N_p - N_n)/N_t]$. The leaf nitrogen contents and partitioning fractions were analysed by multivariate regression against variety, light, nitrogen supply level and leaf age.

### 2.7 Model parameterization

Data obtained in the growth chamber experiment were used to parameterize the dynamics of photosynthetic protein turnover, $R_d$ [see Supporting Information—Fig. S1], and $g_m$ [Supporting Information—Fig. S2). Differential equations (Eqn 1; see Supporting Information—EqnsS1 and S2) were solved in R (version 3.3.0, R Core Team 2019; details see Pao *et al.* 2020) to obtain $S_{pot,X}$, $t_{d,X}$ and $D_{r,X}$. With values of $S_{pot,X}$ [see Supporting Information—Eqn S2] determined for each

factorial combination, coefficients $S_{mm,X}$, $k_{l,X}$ (Eqn 2) and $k_{N,X}$ [see Supporting Information—Eqn S3] were estimated by nonlinear least squares fitting. Relationships between $R_d$ and light [see Supporting Information—Eqn S5], between $g_m$ and $N_p$ [see Supporting Information—Eqns S6 and S7], between $L$ and $t$ (Eqn 6), between $\beta$ and $t$ (Eqn 7), and between $k$ and $L$ (Eqn 8) were also estimated by nonlinear least squares fitting.

### 2.8 In silico Experiment 2—Optimizing photosynthetic nitrogen partitioning

Using cultivar-specific parameters, the model from *in silico* Experiment 1 was used to evaluate the optimality of acclimation strategies of Aramon and SC-50 in coordination with their AC. Simulations were conducted under average DPI during the greenhouse experiment (21.33 mol $m^{-2}$ $d^{-1}$) and also under scenarios of its 0.25- and 2-fold (5.33 and 42.66 mol $m^{-2}$ $d^{-1}$, respectively).

### 2.9 In silico Experiment 3—Exchanging functional acclimation strategy

According to our hypothesis, changing PAS should lead to decreased DCA for a given architecture. To test this, we exchanged PAS between the two varieties while keeping $N_{plant}$ and $N_{leaf}$ unmodified for a given architecture. This resulted only in modifications of the partitioning of $N_p$. Then, DCA was calculated. The relative change in DCA caused by exchanging PAS was calculated in comparison to the DCA under control scenario, where PAS was not exchanged.

## 3. RESULTS

### 3.1 Optimal PAS depends on leaf angle with trade-offs between photosynthetic functions

*In silico* Experiment 1 explored a generalized optimal coordination between PAS (represented by rel$S_{pot,X}$ based on Eqn 2) and AC (represented by various leaf angles ranging between 15° and 75° relative to horizontal, Fig. 2). Following Eqn 5, $k$ decreased (indicating less self-shading and total light interception) with increasing leaf angle (more vertical). To achieve the optimal PAS, nitrogen investment into carboxylation (Fig. 2A) and light harvesting (Fig. 2C) was predicted to be strongly light-dependent. The preference of nitrogen investment to the light harvesting pool increased with reducing light availability and increasing leaf angle (Fig. 2C), the conditions leading to low canopy light interception. The nitrogen investment to carboxylation generally increased with increasing light, and was predicted to be maximized at leaf angles between 50° and 65° (Fig. 2A). On the other hand, the preference of nitrogen investment in electron transport seemed to be also dependent on leaf angle (Fig. 2B), with an intermediate preference and a saturation reached at a lower light level within the angle range of 50°–65°. In this range of leaf angle, the light-dependent trade-off between carboxylation and light harvesting determined the optimal PAS.

### 3.2 Varietal variation in AC

To test if optimal coordination between PAS and AC can be observed in the real-world varieties that were bred under

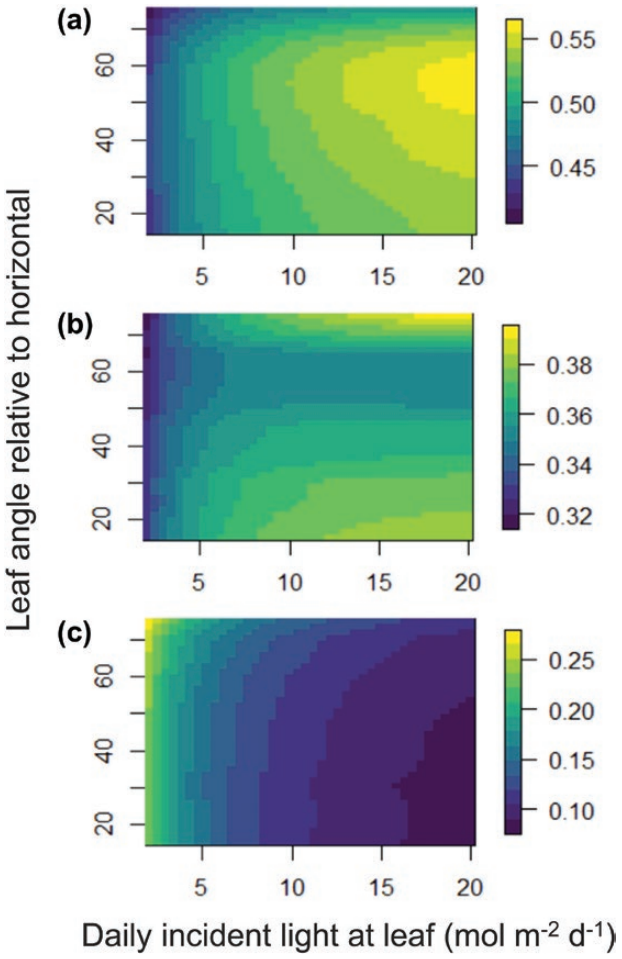


**Figure 2.** Simulated coordination of optimal relative photosynthetic nitrogen synthesis rate with leaf angle (°, $\beta_{abs}$, absolute value of elevation angle) and intercepted DPI, mol $m^{-2}$ $d^{-1}$ in cucumber (*Cucumis sativus* L.). Colours indicate relative potential synthesis rate (rel$S_{pot,op}$) of (A) carboxylation, (B) electron transport and (C) light harvesting protein pools, resulting from theoretically optimal functional acclimation strategy under given leaf angles. The value of $k$ varies with leaf angle following Eqn 5. Variable rel$S_{pot,op,X}$ was calculated as optimized potential synthesis rate ($S_{pot,op,X}$, Eqn 3) divided by the sum of $S_{pot,op,X}$ of all three pools to demonstrate the relative preference of synthesis between the three pools. This simulation was conducted using a virtual cucumber variety with leaf area and functional acclimation coefficients intermediate between Aramon and SC-50, and all leaves in this plant were assumed to have the same leaf angle.

contrasting canopy architecture, we first compared AC visually between the varieties Aramon and SC-50 grown in the greenhouse experiment under single-stem structure. Differences in leaf size and leaf angle were observed (Fig. 1A). From digitized data of the plants, Aramon showed on average 65 % larger single leaf areas ($P < 0.001$) and 17° more vertical leaf angles ($P = 0.005$) than SC-50. We described the AC variation within a canopy by snapshots of the cumulative LAI above a given leaf $L$ (Fig. 1B) and the leaf elevation angle $\beta$ (Fig. 1C) against the thermal age $t$ (°Cd) of the leaves. These traits can be compared between the two varieties due to the comparable phyllochron (°Cd per leaf and thermal time needed for a leaf to appear; Supporting

**Table 1.** Variety-specific coefficients determining AC of cucumber (*Cucumis sativus* L.) cultivars Aramon and SC-50. Standard errors (SE) are indicated in parentheses. Significant differences between varieties at 95 % confidence interval are indicated by lower case letters and ns indicates not significant.

| Description | Eqn | Symbol | Unit | Value (SE) | |
|---|---|---|---|---|---|
| | | | | Aramon | SC-50 |
| LAI above a given leaf | 6 | $L_l$ | – | | |
| Asymptote | | $L_{asym}$ | – | $2.04^{a}$ (0.0845) | $1.23^{b}$ (0.0513) |
| Time at inflection point | | $t_L$ | °Cd | $257.6^{ns}$ (7.25) | $272.1^{ns}$ (7.17) |
| Curve shape coefficient | | $v_L$ | – | $63.9^{ns}$ (3.69) | $63.6^{ns}$ (3.52) |
| Leaf elevation angle | 7 | $\beta$ | ° | | |
| Asymptote | | $\beta_{asym}$ | ° | $-69.2^{ns}$ (3.27) | $-61.1^{ns}$ (3.92) |
| Decrease constant | | $d_\beta$ | $°Cd^{-1}$ | $0.0245^{a}$ (0.00291) | $0.0162^{b}$ (0.00194) |
| Time when decrease begins | | $t_\beta$ | °Cd | $11.0^{b}$ (2.63) | $23.3^{a}$ (3.67) |
| Light extinction coefficient | 8 | $k$ | – | | |
| Maximum | | $k_{max}$ | – | $0.616^{b}$ (0.00277) | $0.853^{a}$ (0.0128) |
| Minimum | | $k_{min}$ | – | $0.359^{ns}$ (0.00516) | $0.337^{ns}$ (0.0270) |
| Leaf area index at maximal $k$ | | $L_k$ | – | $0.286^{a}$ (0.00734) | $0.0846^{b}$ (0.0143) |
| Curve shape coefficient | | $v_k$ | – | $1.089^{b}$ (0.0388) | $1.708^{a}$ (0.186) |

Information—Eqns S15 and S16, Fig. S3) between the varieties. In both varieties, $L$ followed a logistic function with $t$ (Fig. 1B, Eqn 6) and approached an asymptote $L_{asym}$ equivalent to the LAI of the canopy at the end of the greenhouse experiment, where Aramon showed 66 % higher $L_{asym}$ than SC-50 (Table 1). In a plant, new leaves emerge in a vertical orientation from the tip, and then turn gradually downwards along their expansion, resulting in a temporal change in the elevation angle. This process starts when the leaf reaches an age of $t_\beta$ (°Cd), thereafter the leaf turns downward by a rate constant $d_\beta$ ($°Cd^{-1}$) and remains at a more or less stable value of $\beta_{asym}$ (°, Fig. 1C, Eqn 7) after fully expansion. The values of $\beta_{asym}$ of the two varieties range between −60° and −70° (Fig. 1c), and were not significantly different (Table 1). The negative values of $\beta_{asym}$ indicate a downward direction from the horizontal plane. Since $\cos(-\beta) = \cos(\beta)$ in the cosine correction for light interception [see Supporting Information—Eqn S13], in the following $\beta$ will be discussed in its absolute value $\beta_{abs}$ for simplicity. The 34 % lower $d_\beta$ of SC-50 (Table 1) indicates that its leaves turn downwards at a slower rate, leading to a more horizontal (smaller values of $\beta_{abs}$) angle distribution at the upper canopy layer (Fig. 1C) and at earlier canopy developmental stages (Fig. 3) where the canopy consists of a higher proportion of leaves that are not yet fully expanded.

### 3.3 Architectural variation leads to different light distribution in the canopy

To quantify the intra-canopy light distribution, digitized data were used to first reconstruct virtual plants. By coupling a light model to the virtual canopies, light transmission through the canopies was simulated to determine light extinction coefficients ($k$) at the different canopy developmental stages [see Supporting Information—Methods S1]. The variation in $k$ with canopy development (Fig. 4), likely due to the change of leaf angle distribution (Fig. 3), was represented by a log-normal function of LAI ($L$, Eqn 8), where a minimal light extinction coefficient $k_{min}$, and a maximal light extinction coefficient $k_{max}$ occurring at a canopy LAI of $L_k$ were specified. The higher $k$ of SC-50 canopies during the early developmental stages (Fig. 4) is mainly due to its 38.5 % higher $k_{max}$ compared to Aramon (Table 1). This agrees with the general understanding that, for a given LAI, canopies with horizontal angle distribution (Fig. 3) are associated with high $k$ (Monsi and Saeki 2005).

### 3.4 General acclimatory responses of leaf nitrogen contents to light intensity, nitrogen supply and leaf age

Light acclimation of leaf nitrogen content and partitioning were measured on leaves grown in a controlled environment, where the sampled leaves were fixed perpendicularly to the incident light in order to exclude the effects of leaf angle and to avoid shading from other leaves. Under constant light intensities, the total leaf nitrogen $N_t$, photosynthetic nitrogen $N_p$ and the nitrogen in the three functional nitrogen pools (carboxylation, $N_V$, electron transport, $N_J$, and light harvesting, $N_C$) were examined see [Supporting Information—Fig. S4]. Multivariate regression analyses were conducted to disentangle the effects of variety, light, leaf age, nitrogen supply on the leaf nitrogen contents, and to identify the variety-specific responses. It was found that these factors and interactions together explained 44 %–73 % of the variation in the nitrogen contents of various functional pools (Table 2).

Common positive responses of the nitrogen contents to light [see Supporting Information—Fig. S4] and to nitrogen supply were observed in both varieties (Table 2) without significant varietal interactions with the both factors. No significant difference between varieties was found in $N_t$, $N_p$, $N_V$, $N_J$ and $N_C$ content in the leaves (Table 2). Interestingly, there was an interaction between variety and leaf ageing. In the leaves of Aramon, $N_t$ and $N_p$ (mainly through $N_C$) increased with leaf development while $N_J$ decreased slightly (Table 2). In the case of SC-50, $N_t$ increased to a greater extent along leaf development while $N_p$ decreased (Table 2).

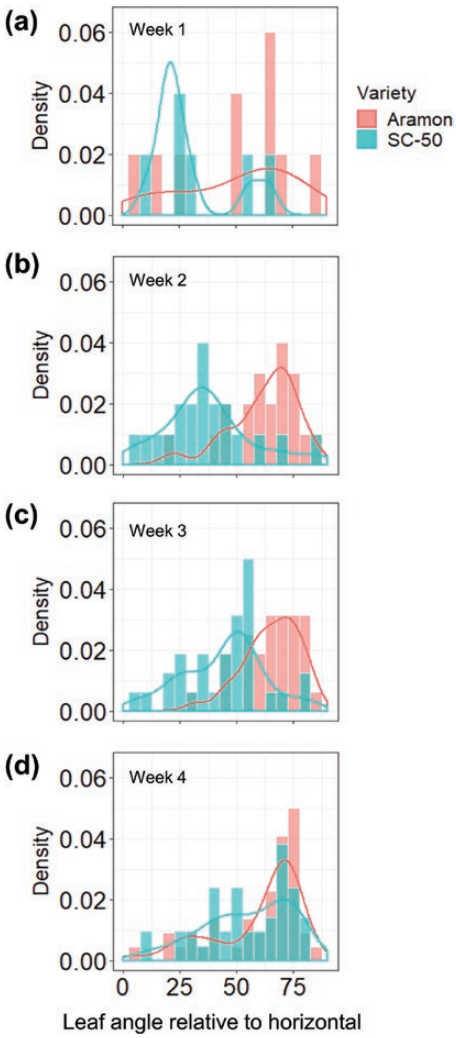


**Figure 3.** Leaf angle (°, absolute value of elevation angle and relative to horizontal) distribution of cucumber (*Cucumis sativus* L.) cultivars Aramon and SC-50 measured in four consecutive weeks using digitization. Measured leaf angle at the (A) First, (B) second, (C) third and (D) fourth week. Absolute values of leaf elevation angles are shown. An angle distribution with high density of large leaf angle is characterized as vertical leaf angle distribution (erectophile), otherwise horizontal leaf angle distribution (planophile).

### 3.5 Varietal variation in light response of leaf nitrogen partitioning

According to our hypothesis, plants should develop PAS to coordinate $N_p$ partitioning with light intensity. The partitioning of $N_t$ and $N_p$ into different pools was quantified (Fig. 5). Significant interactions between light and variety were found using multivariate analyses, where the factors tested explained 39 %–60 % of the variation in the nitrogen partitioning fractions (Table 3).

Among the varieties, only Aramon showed a light response with respect to the partitioning of $N_t$ (Fig. 5A–C), such that the proportion of leaf nitrogen invested into photosynthesis ($p_{Np}$) decreased with increasing incident light (−0.45 % per mol photon $m^{-2}$ $d^{-1}$, Table 3, Fig. 5A). In addition, with increasing light, the fraction of $N_t$ invested in nitrate ($p_{Nn}$) also decreased (−0.23 % per mol photon $m^{-2}$ $d^{-1}$, Fig. 5C), while the fraction of

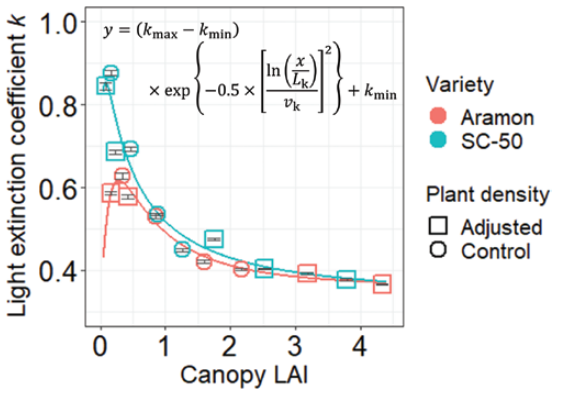


**Figure 4.** Relationship between light extinction coefficient ($k$) and canopy LAI. $k$ is fitted (lines) to a function of canopy LAI ($L_c$, Eqn 8) to include developmental and density effects incucumber (*Cucumis sativus* L.) cultivars Aramon and SC-50. Data with standard errors were results of ten independent simulations of light transmission to the ground obtained using static 3D virtual canopies in GroIMP, sampled from the ground area under the five middle plants in the central row of the canopy (Fig. 1D). Plant density in the simulations was set either to 1.33 plants $m^{-2}$ as in the greenhouse experiment (circles, control) or to 0.5-, 2- or 3-fold of that in the greenhouse experiment (squares, adjusted) by proportionally adjusting both distances between rows and between plants in a row.

$N_t$ invested in structure and functions other than photosynthesis ($p_{Nf}$) increased in the leaves of Aramon (+0.74 % per mol photon $m^{-2}$ $d^{-1}$, Table 3, Fig. 5B). SC-50 invested generally less nitrogen in photosynthesis than Aramon (lower $p_{Np}$ by 11.5 %, Table 3, Fig. 5A) but more in structure and functions other than photosynthesis (higher $p_{Nf}$ by 21.6 %, Fig. 5B, Table 3). Increasing nitrogen supply resulted in decreased $p_{Np}$ and increased $p_{Nn}$ in both varieties (Table 3).

Both varieties developed qualitatively similar light acclimation strategies in the partitioning of $N_p$, such that the fractions of $N_p$ partitioned to $N_V$ ($p_V$) and $N_J$ ($p_J$) increased with incident light (Fig. 5D and E), while that to $N_C$ ($p_C$) decreased (Fig. 5F). However, there were quantitative differences in the light response between varieties (Table 3). In comparison to Aramon, SC-50 showed 2.42 % lower $p_J$ and 4.30 % higher $p_C$ under low light availability (Table 3), suggesting a preference of SC-50 to invest $N_p$ in light harvesting at the expense of electron transport under light-limiting conditions. Interestingly, SC-50 showed significantly higher sensitivity to light in $p_V$ and $p_C$ (steeper slopes in Fig. 5D and F, Table 3), resulting in trends of higher $p_V$ and lower $p_C$ under high light availability (DPI > 20 mol $m^{-2}$ $d^{-1}$) in SC-50 than in Aramon (Fig. 5D and F). Significant effects of nitrogen supply on the partitioning of $N_p$ were not evident in both varieties (Table 3), but a shift from $p_J$ to $p_C$ could be observed as leaves aged (Table 3).

### 3.6 Varietal variation in photosynthetic protein synthesis

We further used a mechanistic model of photosynthetic protein turnover (Eqns 1 and 2) to explain the observed variation in PAS between varieties. In the model, genetic controls of PAS were characterized by three parameters: maximum protein synthesis rate $S_{mm}$, decrease constant of synthesis rate with

**Table 2.** Multivariate regression analysis of the effects of cucumber (*Cucumis sativus* L.) varieties (V) Aramon and SC-50, daily light interception (I, mol $m^{-2}$ $d^{-1}$), nitrogen supply level (N, mM), and leaf age (A, °Cd) on nitrogen components, total leaf nitrogen ($N_t$), photosynthetic nitrogen ($N_p$), nitrogen invested in carboxylation ($N_V$), electron transport ($N_J$) and light harvesting ($N_C$) functions. The data were analysed by the model: Variable ~ I + N + A. The coefficients of each factor were determined for both varieties. Asterisks indicate the statistical significance of the coefficients for Aramon, whereas for SC-50 the asterisks indicate the significance of differences in the coefficients from those of Aramon. Standard errors of the coefficients are shown in parentheses. Adjusted *R*-squared ($R^2_{adj}$) values for each analysis are shown.

| Variety | Aramon | | | | SC-50 | | | | $R^2_{adj}$ |
|---|---|---|---|---|---|---|---|---|---|
| Effect | V | I | N | A | V | I | N | A | |
| $N_t$ (mmol $m^{-2}$) | 31.5** | 4.77*** | 5.37*** | 0.0574* | 19.0$^{ns}$ | 4.79$^{ns}$ | 3.76$^{ns}$ | 0.191*** | 0.73 |
| | (10.1) | (0.299) | (0.998) | (0.0237) | (15.0) | (0.451) | (1.41) | (0.0333) | |
| $N_p$ (mmol $m^{-2}$) | 34.5*** | 1.18*** | 0.742* | 0.0180* | 29.2$^{ns}$ | 1.16$^{ns}$ | 0.777$^{ns}$ | −0.0171** | 0.59 |
| | (3.79) | (0.112) | (0.374) | (0.00886) | (5.42) | (0.167) | (0.527) | (0.0122) | |
| $N_V$ (mmol $m^{-2}$) | 12.9*** | 0.615*** | 0.385* | 0.00742$^{ns}$ | 10.9$^{ns}$ | 0.634$^{ns}$ | 0.312$^{ns}$ | −0.00748* | 0.61 |
| | (1.80) | (0.0532) | (0.177) | (0.00421) | (2.57) | (0.0793) | (0.250) | (0.00580) | |
| $N_J$ (mmol $m^{-2}$) | 11.6*** | 0.460*** | 0.209$^{ns}$ | −0.00640* | 8.98$^{ns}$ | 0.434$^{ns}$ | 0.271$^{ns}$ | −0.0128$^{ns}$ | 0.61 |
| | (1.35) | (0.0400) | (0.133) | (0.00316) | (1.93) | (0.0597) | (0.188) | (0.00436) | |
| $N_C$ (mmol $m^{-2}$) | 10.0*** | 0.105*** | 0.148$^{ns}$ | 0.0169*** | 9.38$^{ns}$ | 0.0963$^{ns}$ | 0.194$^{ns}$ | 0.00300*** | 0.44 |
| | (1.01) | (0.0299) | (0.0998) | (0.00237) | (1.45) | (0.0446) | (0.141) | (0.00326) | |

*$P < 0.05$; **$P < 0.01$; ***$P < 0.001$; $^{ns}$not significant.

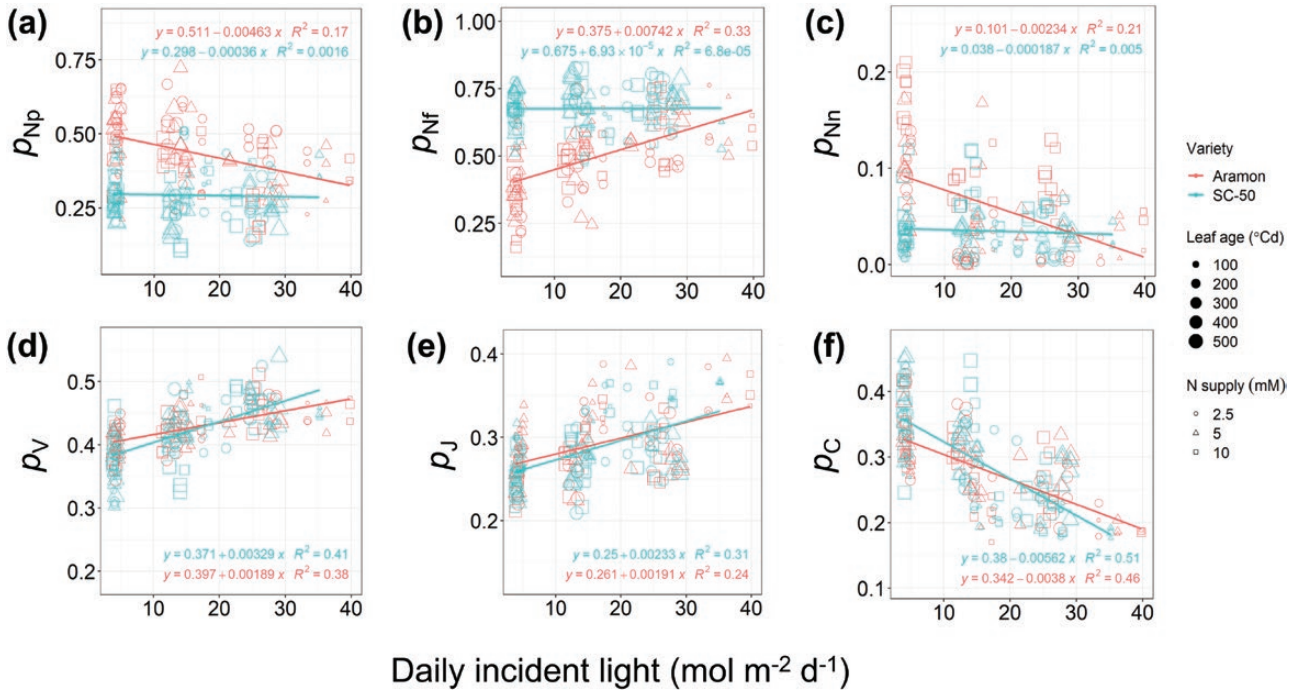


**Figure 5.** Measured nitrogen partitioning fractions in leaves of different ages under different daily incident light and nitrogen supply. (A) Photosynthetic nitrogen in total leaf nitrogen ($p_{Np}$), (B) organic nitrogen in functions other than photosynthesis in total leaf nitrogen ($p_{Nf}$), (C) nitrate-nitrogen in total leaf nitrogen ($p_{Nn}$), fractions of photosynthetic nitrogen invested in (D) carboxylation ($p_V$), (E) electron transport ($p_J$), (f) light harvesting ($p_C$). Data were obtained in the growth chamber experiment. Linear regressions (lines) and their *R*-squared values for cucumber (*Cucumis sativus* L.) cultivars Aramon and SC-50 are shown. Leaf age is indicated by symbol size and nitrogen supply level by different symbols.

age $t_d$, and protein degradation constant $D_r$ [see Supporting Information—Table S3]. Coefficients $t_d$ and $D_r$ together influence the developmental effect on protein turnover dynamics (Eqn 1; see Supporting Information—Eqn S2). Coefficient $D_r$ was assumed the same for both cultivars Aramon and SC-50, with values estimated in our previous study (Table 1 in Pao *et al.* 2019a). Higher $S_{mm}$ of Aramon [see Supporting Information—Table S3] suggests that its photosynthetic protein synthesis can reach a higher rate (maximal differences of 0.1, 0.06 and 0.02 mmol °$Cd^{-1}$ $m^{-2}$ for $N_V$, $N_J$ and $N_C$, respectively), while its lower $t_d$ indicates that the influence of ageing appears later in its leaves' lifespan than in the leaves of SC-50. These together led to higher

**Table 3.** Multivariate regression analysis of the effects of cucumber (*Cucumis sativus* L.) varieties (V) Aramon and SC-50, daily light interception (I, mol $m^{-2}$ $d^{-1}$), nitrogen supply level (N, mM), and leaf age (A, °Cd) on nitrogen components, fraction of photosynthetic nitrogen ($N_p$) in total leaf nitrogen ($p_{Np}$), fraction of organic nitrogen in other functioning other than photosynthesis in total leaf nitrogen ($p_{Nf}$), fraction of inorganic nitrate-nitrogen in total leaf nitrogen ($p_{Nn}$), fractions of $N_p$ invested in carboxylation ($p_V$), in electron transport ($p_J$) and in light harvesting ($p_C$). The data were analysed by the model: Variable ~ I + N + A. The coefficients of each factor were determined for both varieties. Asterisks indicate the statistical significance of the coefficients for Aramon, whereas for SC-50 the asterisks indicate the significance of differences in the coefficients from those of Aramon. Standard errors of the coefficients are shown in parentheses. Adjusted *R*-squared ($R^2_{adj}$) values for each analysis are shown.

| Variety | Aramon | | | | SC-50 | | | | $R^2_{adj}$ |
|---|---|---|---|---|---|---|---|---|---|
| Effect | V | I | N | A | V | I | N | A | |
| $p_{Np} \times 100$ | 54.6*** | −0.452*** | −0.824** | 0.00433$^{ns}$ | 43.1** | −0.103** | −0.213$^{ns}$ | −0.0400*** | 0.51 |
| | (2.82) | (0.0832) | (0.278) | (0.00658) | (4.16) | (0.125) | (0.393) | (0.00925) | |
| $p_{Nf} \times 100$ | 37.3*** | 0.744*** | −0.0360$^{ns}$ | 0.00155$^{ns}$ | 58.9*** | 0.0830*** | −0.307$^{ns}$ | 0.0331** | 0.59 |
| | (3.12) | (0.0888) | (0.296) | (0.00723) | (4.64) | (0.135) | (0.421) | (0.0102) | |
| $p_{Nn} \times 100$ | 4.19*** | −0.234*** | 0.899*** | 0.00218$^{ns}$ | −1.10*** | 0.00200*** | 0.522** | 0.00537$^{ns}$ | 0.54 |
| | (1.01) | (0.0287) | (0.0958) | (0.00234) | (1.50) | (0.0436) | (0.136) | (0.00328) | |
| $p_V \times 100$ | 39.1*** | 0.188*** | 0.105$^{ns}$ | −0.000059$^{ns}$ | 37.2$^{ns}$ | 0.329** | −0.0180$^{ns}$ | −0.000249$^{ns}$ | 0.39 |
| | (1.02) | (0.0302) | (0.101) | (0.00239) | (1.46) | (0.0451) | (0.142) | (0.00330) | |
| $p_J \times 100$ | 31.4*** | 0.172*** | −0.0332$^{ns}$ | −0.0183*** | 29.0* | 0.217$^{ns}$ | 0.0440$^{ns}$ | −0.0151$^{ns}$ | 0.58 |
| | (0.821) | (0.0243) | (0.0810) | (0.00192) | (1.17) | (0.0362) | (0.114) | (0.00265) | |
| $p_C \times 100$ | 29.4*** | −0.360*** | −0.0715$^{ns}$ | 0.0184*** | 33.7* | −0.546** | −0.0259$^{ns}$ | 0.0154$^{ns}$ | 0.60 |
| | (1.35) | (0.0398) | (0.133) | (0.00315) | (1.93) | (0.0594) | (0.187) | (0.00434) | |

*$P < 0.05$; **$P < 0.01$; ***$P < 0.001$; $^{ns}$not significant.

amounts of $N_p$ observed in the leaves of Aramon [see Supporting Information—Fig. S4B–D].

Genotypic sensitivities to light and nitrogen availabilities are denoted by $k_I$ and $k_N$, respectively. These coefficients determine the sensitivity of potential maximum protein synthesis rates $S_{pot}$ (Eqn 2) to increasing light and nitrogen availabilities until reaching their maximum $S_{mm}$ (Fig. 6A). Relative potential synthesis rate rel$S_{pot}$, calculated by dividing the potential synthesis rate of a pool *X*, $S_{pot,X}$, by the sum of $S_{pot}$ of all three pools (Fig. 6B), suggested that $N_p$ partitioning to both carboxylation and electron transport pools increased non-linearly with light, while partitioning to light harvesting decreased. The difference in rel$S_{pot}$ between the varieties was apparent below DPI ≤ 20 mol $m^{-2}$ $d^{-1}$, where simulations showed that Aramon invested higher proportions of $N_p$ to carboxylation and electron transport pools than to the light harvesting pool in comparison to SC-50 (Fig. 6C). This is in accordance with observations (Fig. 5D–F).

### 3.7 Optimality and flexibility of light acclimation in combination with plant architecture

Parameterization of variety-specific functional and architectural parameters allows evaluation of the degree of coordination between PAS and AC. For both varieties, the single-stem architecture was applied in the *in silico* Experiment 2 under various plant densities. The theoretically optimal PAS that yields the $N_p$ partitioning pattern which maximizes daily carbon assimilation (DCA, mol $CO_2$ $d^{-1}$ per plant) was identified under various daily photosynthetic photon integrals (DPIs), and the index of optimality (%) was determined using Eqn 4. The optimality was shown over 87 % for all the plant densities (1.33 and 3.99 plants $m^{-2}$) and DPI levels (6.4–42.6 mol $m^{-2}$ $d^{-1}$) tested (Fig. 7). Under a plant density of 1.33 plants $m^{-2}$ as in the greenhouse experimental setup, optimal PAS was found under DPI levels between 8 and 27 mol $m^{-2}$ $d^{-1}$ for Aramon, and between 8 and 13 mol $m^{-2}$ $d^{-1}$ for SC-50 (Fig. 7A). The PAS of Aramon ($PAS_{Aramon}$) was optimal under the average DPI level during the greenhouse experiment (21.33 mol $m^{-2}$ $d^{-1}$), indicating its ability to maximize DCA by acclimatizing $N_p$ partitioning to its growing light environment. However, this was not the case for SC-50, the variety having a lower amount of $N_p$ [see Supporting Information—Fig. S4B–D] despite of a PAS that was more sensitive to light (Table 3). Aramon's higher adaptability to high light conditions can be expected from its higher amount of $N_p$ (Table 2, see Supporting Information—Fig. S4B–E). Virtual scenarios of higher plant densities were tested to simulate the conditions with denser canopies. Interestingly, under a 3-fold density (3.99 plants $m^{-2}$), SC-50 exhibited a wider DPI range where its PAS was optimal (6–16 mol $m^{-2}$ $d^{-1}$) in comparison to that at a plant density of 1.33 plants $m^{-2}$, while the performance of Aramon did not show any apparent change, except for a 4.8 % decrease under the lowest DPI level tested (Fig. 7B).

### 3.8 The variety-specific combination of PAS and AC was not always optimal but SC-50's PAS ameliorates the impact of strong light competition

According to our second hypothesis, if a variety has a PAS that ideally coordinates with its AC, modifications of PAS should lead to reduced DCA for a given architecture. To test this, DCA was simulated by combining the PAS of one variety with the AC of the other in *in silico* Experiment 3 under various planting densities and light regimes. In contrast to our expectation, combining PAS of a cultivar with AC of another cultivar did not result in a constant decrease of DCA (Fig. 8). The optimal combination

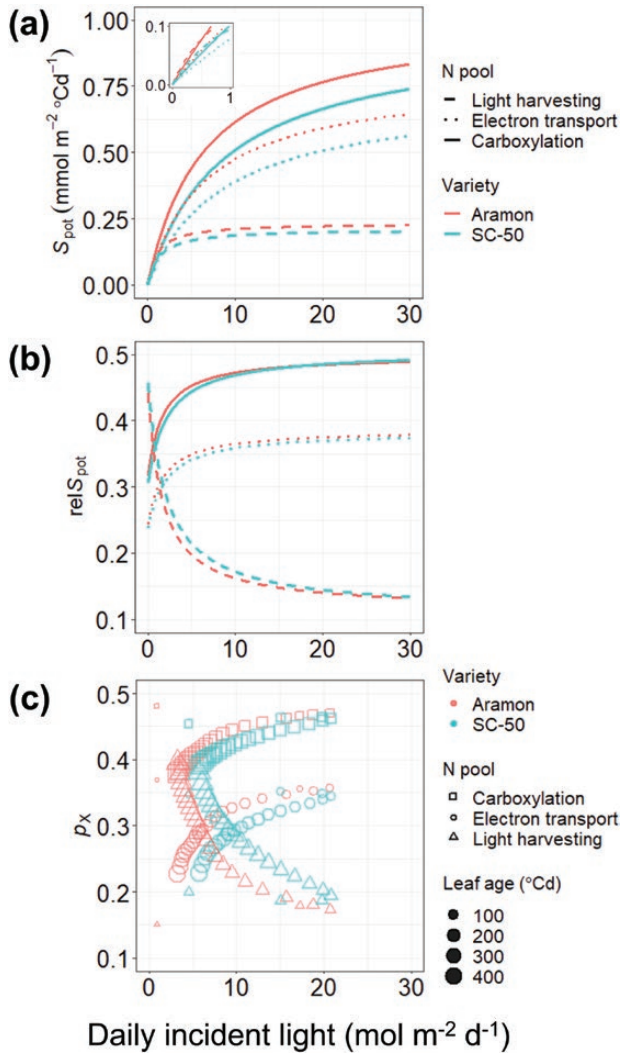


**Figure 6.** Simulated light acclimation of photosynthetic nitrogen in cucumber (*Cucumis sativus* L.) cultivars Aramon and SC-50. (A) Potential protein synthesis rates ($S_{pot}$, mmol N m$^{-2}$ °Cd$^{-1}$) for carboxylation (solid lines), electron transport (dotted lines) and light harvesting (dashed lines) and the resulting (B) relative potential synthesis rates (rel$S_{pot}$) in response to daily incident light. The rates under incident light of 1 mol m$^{-2}$ d$^{-1}$ is shown in the insertion. These simulations were conducted with a nitrogen supply level of 10 mM $NO_3^-$. (C) Photosynthetic nitrogen partitioning fractions ($p_X$) of carboxylation (squares), electron transport (circles) and light harvesting (triangles) for individual leaves of a plant. Leaf age is indicated by symbol size. This simulation was conducted with incident light of 21.33 mol m$^{-2}$ d$^{-1}$ and plant architecture digitized in the fourth week of the greenhouse experiment.

between PAS and AC was rather dynamic depending on canopy development. This effect was marginal (<5 %, Fig. 8) but appeared to vary with DPI level and planting density. High planting density (2.66 plants m$^{-2}$) and low DPI (5.33 mol m$^{-2}$ d$^{-1}$) led to strong inter-plant light competition, where the advantageous effect of SC-50's PAS ($PAS_{SC-50}$) became more pronounced (Fig. 8A). In contrast, the reduction in DCA of SC-50 architecture caused by $PAS_{Aramon}$ aggravated under low DPI (Fig. 8D). This suggested that $PAS_{SC-50}$ ameliorated the impact of strong light competition, while $PAS_{Aramon}$ did not.

## 4. DISCUSSION

Plants can be expected to develop PAS according to their AC) either through natural evolution or artificial selection, to coordinate nitrogen use with local light availability. To the best of our knowledge, we report here varietal variation in PAS (Figs. 5 and 6) together with AC (Figs. 1 and 3) for the first time. We also interpret these variations in the context of optimal coordination of PAS with AC (Figs. 7 and 8) using a modelling approach and derive a generalized coordination between PAS and AC (Fig. 2).

### 4.1 Co-evolution between photosynthetic acclimation and architecture-dependent degree of light competition

Despite the differences in AC and PAS, the two studied varieties are comparably vigorous in vegetative growth [see Supporting Information—Figs. S3 and S5] and highly productive under their conventional cultivation conditions (Papadopoulos and Hao 2000; Shetty and Wehner 2002). One would expect that these cultivars optimize PAS according to light availability and to their respective AC as is reported for other species (Evans 1993b; Hikosaka and Terashima 1996). Our simulations suggested that the greenhouse cultivar Aramon had an optimal PAS under the growing light conditions (21.3 mol m$^{-2}$ d$^{-1}$) of a vertical greenhouse training system (Fig. 1A), while this was not the case for the field varieties SC-50 (Fig. 7), which was selected for a creeping multi-branching 'canopy'. Simulations suggested that $PAS_{SC-50}$ appeared to be more efficient under light competition either due to low light or high plant density (Figs. 7B and 8), suggesting that not $PAS_{SC-50}$ per se is sub-optimal but the combination of $PAS_{SC-50}$ and the single-stem architecture.

The variation in functional traits could be interpreted as a result of their co-evolution with canopy AC during breeding under specific cultivation conditions. Based on our findings, we propose a scheme presenting how breeding background might have affected the coordination between functional and AC (Fig. 9). Aramon is a parthenocarpic and gynoecious cultivar bred for vertical single-stem training systems in the greenhouse, where environmental conditions are often free from stress. In contrast, SC-50 is a monoecious cultivar bred in a creeping form under open-field conditions, where biotic and abiotic stresses occur more frequently. The sex determination of a cultivar can determine the canopy form preferred under a yield-driven breeding process. SC-50 is monoecious and its female flowers appear predominantly on the lateral shoots, so it was bred in a multi-stem form. Such a canopy form leads consequently to stronger intra-canopy shading. Furthermore, SC-50 has generally more horizontal leaves (Fig. 3), which further aggravates self-shading (but increases overall canopy light interception). In contrast, Aramon is bred under vertical single-stem culture and has more vertical leaves than SC-50 (Niklas and Hammond 2013). To cope with self-shading, SC-50 develops (i) a PAS with higher sensitivity to light intensity helps optimize the nitrogen investment, thereby maintaining PNUE (Fig. 9) and (ii) horizontal leaf orientation and high $k$ to gain advantage under light competition (Schieving and Poorter 1999; Hikosaka and Hirose 1997).

Both varieties had comparable amounts of total leaf nitrogen (Table 2), but SC-50 invested less leaf nitrogen in photosynthesis regardless of light environment (Table 3, Fig. 5A). Presumably due to the high total light interception of SC-50 canopies in the

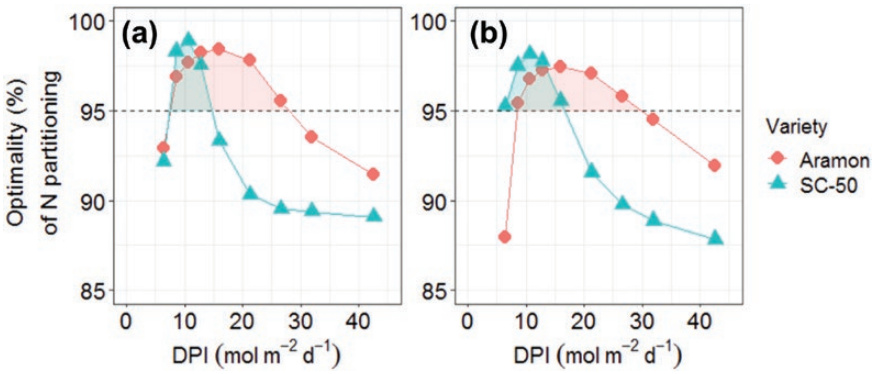


**Figure 7.** Simulated optimality of functional acclimation strategy (PAS) under various incident DPIs, mol photon $m^{-2}$ $d^{-1}$. Simulations were conducted at a plant density of (A) 1.33 and (B) 3.99 plants $m^{-2}$ for cucumber (*Cucumis sativus* L.) cultivars Aramon (circles) and SC-50 (triangles), using architectures digitized in the fourth week of the greenhouse experiment, where the average DPI during the whole growth period was 21.33 mol $m^{-2}$ $d^{-1}$. PAS is represented by function-specific response of protein synthesis rate to light and the resulting partitioning of photosynthetic nitrogen. The optimality is quantified as the relative differences in daily carbon assimilation (DCA, mol $d^{-1}$ per plant) between the theoretically optimal PAS and variety-specific PAS. An optimality level over 95 % (dashed lines) suggests an optimal PAS under a given DPI.

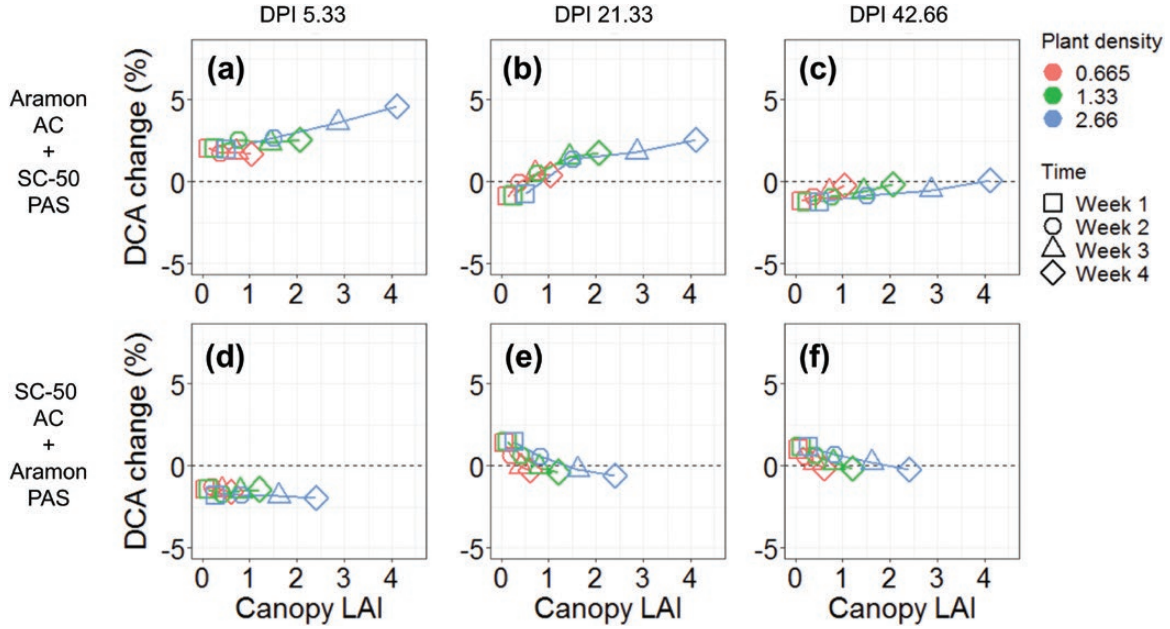


**Figure 8.** Simulated effect of combining PAS of one variety with AC of the other on daily carbon assimilation of cucumber (*Cucumis sativus* L.) varieties. PAS is represented by the response of photosynthetic nitrogen partitioning to light. Relative change in DCA as compared within a given architecture, either (A)–(C) Aramon or (D)–(F) SC-50. Plant densities of 0.665, 1.33 and 2.66 plants $m^{-2}$ ground were used in the simulations in combination with incident DPIs of 5.33 [(A), (D)], 21.33 [(B), (E)] and 42.66 mol $m^{-2}$ $d^{-1}$ [(C), (F)], for architectures digitized in four consecutive weeks as indicated by different symbols.

open-field, photosynthesis is less of a limitation for productivity than the stresses in the environment. In this case, SC-50 may prioritize nitrogen investment in other chemical compounds (Table 3, Fig. 5B), for example in structural strength and defense against biotic (e.g. downy mildew and anthracnose; Criswell *et al.* 2010) and abiotic stresses (Strauss-Debenedetti and Bazzaz 1991; Hikosaka, 2004; Onoda *et al.* 2004; Poorter *et al.* 2009), which is especially crucial under inter-plant competition (de Vries *et al.* 2018). Plants benefit from higher robustness at the expense of reduced investment in photosynthesis and growth as long as the costs of defense mechanisms do not outweigh the benefits of reduced damage (Tian *et al.* 2003; Dalin *et al.* 2010; Todesco *et al.* 2010). In addition, the effect of less relative nitrogen investment in photosynthesis in SC-50's leaves is partly compensated by its higher sensitivity of $N_p$ partitioning to light intensity (Fig. 5D and F, Table 3) to improve the use efficiency of $N_p$. In contrast to SC-50, Aramon can afford to invest more nitrogen in photosynthesis under greenhouse conditions and adjust its proportion flexibly according to the light conditions (Fig. 5A, Table 3). Aramon showed increased relative investment of total nitrogen in photosynthesis with decreasing light availability (Fig. 5A), ensuring stable performance over a wider range of light

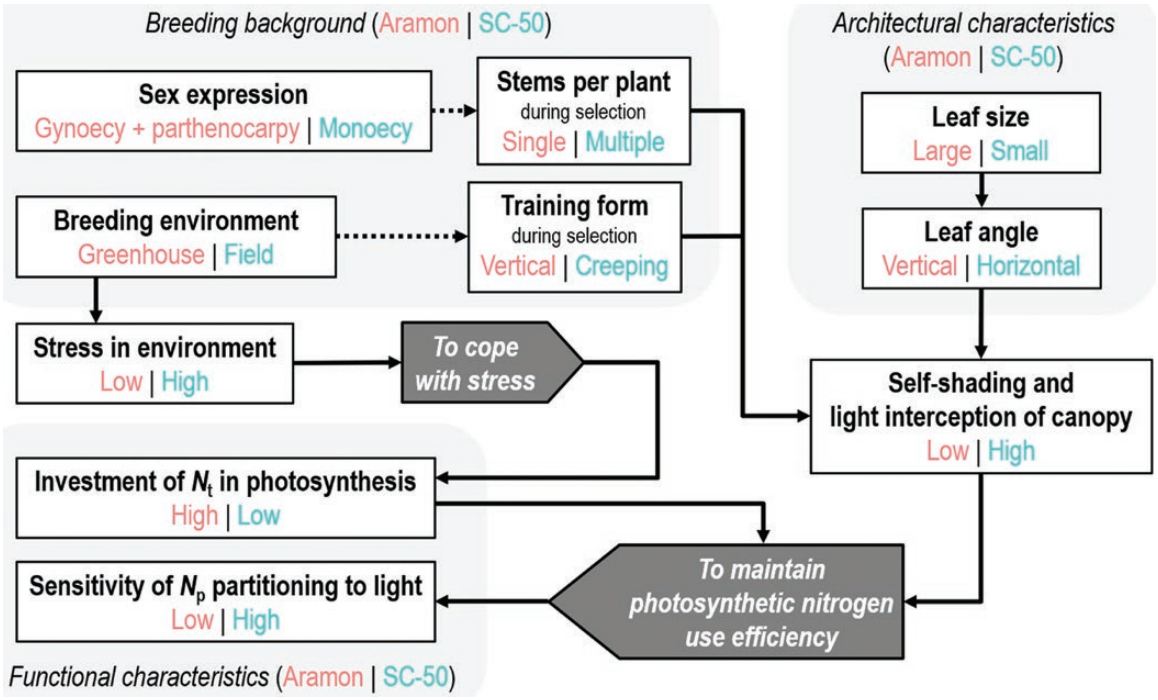


**Figure 9.** Proposed scheme of the influence of breeding background on the development of coordination between functional and AC. $N_t$ and $N_p$ denote total leaf nitrogen and photosynthetic nitrogen, respectively. The characteristics of for their breeding background, architecture and function are shown for varieties Aramon and SC-50. Solid arrows indicate cause and effect relationships.

intensities, particularly under light limiting conditions, the usual situation in greenhouses. However, this partitioning strategy can restrain the further increase in photosynthetic capacity under high light conditions. This complies with a 'generalization' strategy that provides a moderate fitness over a wide range of environments (DeWitt and Langerhans 2004; Sadras and Richards 2014). This strategy results in the stable photosynthetic performance of Aramon between seasons in comparison with SC-50 in a greenhouse experiment [see Supporting Information—Fig. S5A], and also the stable optimality in PAS between different plant densities (Fig. 7).

### 4.2 Optimal coordination between photosynthetic nitrogen partitioning and leaf angle

Apart from the varietal coordination between PAS and AC, we derived a generalized pattern of coordination between PAS and leaf angle that led to maximal plant carbon assimilation (Fig. 2). Modification in leaf angle either increases or decreases self-shading and total light interception simultaneously. Since nitrogen investment in Rubisco is predicted to be higher under conditions with excessive energy supply (e.g. Yin *et al.* 2019), our simulation suggests maximal light interception at 50°–65° in the virtual canopies (Fig. 2A). Following the predicted optimal PAS, the reduction of canopy light interception caused by leaf angles deviating from this angle range is compensated by an increase in nitrogen investment in electron transport (Fig. 2B). Intra-canopy light variation caused either by shading or incoming light conditions are coped with through the nitrogen partitioning between carboxylation and light harvesting (Fig. 2A and C) for keeping the PNUE constant by allocating nitrogen to limiting function (Evans 1993a; Hikosaka 2004; Buckley *et al.* 2013; Pao *et al.* 2019a; Yin *et al.* 2019). Under conditions of high incident light combined with horizontal leaves, a preference in investment in electron transport instead of light harvesting (Fig. 2B and C) provides theoretically an advantage over photoinhibition (although not implemented in the current model) by balancing light absorption and photochemistry (Murchie and Niyogi 2011). This is achieved by (i) reducing the amount of light-harvesting complexes per photosystem II to avoid excessive energy absorption and (ii) maintaining adenosine triphosphate (ATP) production to support photosystem II integrity (Bailey *et al.* 2001; Murata *et al.* 2007). In order to optimize the use of a limited budget of available leaf nitrogen for plant fitness and robustness, the trade-off in nitrogen allocation between functions is predictable (Hikosaka and Terashima 1996; Buckley *et al.* 2013; Pao *et al.* 2019a) and has been widely reported in photosynthetic acclimation (Evans 1988, 1989; Onoda *et al.* 2004; Hikosaka 2005; Muller *et al.* 2005; Trouwborst *et al.* 2011; Evans and Clarke 2019) mainly through post-transcriptional regulation which takes place within hours after exposure to a change in light (Mettler *et al.* 2014; Miller *et al.* 2017). Yet the degree of this trade-off varies depending on environments and may tilt towards electron transport in the future since rising ambient $CO_2$ concentration and temperature can lead to more frequent limitation of photosynthesis by RuBP regeneration under saturating light (Long *et al.* 2004; Taylor *et al.* 2020).

### 4.3 Model assumptions and limitations

The model presented here integrates both architectural and functional processes from leaf to canopy level and enables *in silico* experiments and optimizations which could not be realized

experimentally. Although more complexity might not necessarily lead to improved comprehension under the context of our research question, there are at least three aspects worth noting.

First, we simplified AC by using the light extinction coefficient, estimated by 3D canopy architecture model with considerations of canopy dynamics (Eqns 8; see Supporting Information—Eqns S13 and S14) as a proxy for canopies consisting of a single variety. It can be argued that higher realism regarding heterogeneity of light distribution (e.g. differentiating sunlit and shaded leaves in each layer of the canopy) should be also considered for better insight into canopy nitrogen use (de Pury and Farquhar 1997; Hikosaka 2014). However, we would like to emphasize that increasing the number of parameters representing AC using 3D-model makes it impossible to derive a generalized coordination between PAS and AC (Fig. 2), hampering the iterative optimization algorithm and reducing the chance to obtain a global optimum. Although fine adaptations in intra-canopy light distribution through leaf light reflectance and absorptance (e.g. Song *et al.* 2017), tropism and shade avoidance behaviour (Maddonni *et al.* 2001a; Kahlen *et al.* 2008; Kahlen and Stützel 2011) and the potential issues related to the interactive effects between sun angle and leaf angles on light extinction coefficient cannot be examined explicitly with the model presented in this paper, the accuracy in predicting photosynthetic parameters at leaf level is reasonable (Pao *et al.* 2019a) and at the canopy level, similar to that using a dynamic functional-structural plant model (Pao *et al.* 2021).

Second, area-based $N_p$ was directly simulated in our model (Eqn 1) to facilitate the understanding in photosynthetic acclimation due to its relation to light interception per leaf area. It should be noted that, the intrinsic relationship between leaf mass per area (LMA) and mass-based $N_p$ (Wright *et al.* 2004) is implicitly included. Additionally, LMA shows similar nonlinear pattern of light acclimation (Poorter *et al.* 2009) as that proposed for $N_p$, implying that the change in PUNE following light acclimation can be a mixed outcome of modification in nitrogen economics and in dry mass investment per area (Hikosaka 2004). Therefore, although the protein level of the light harvesting pool actually decreases after exposure to increasing light and photoperiod (Bailey *et al.* 2001; Mettler *et al.* 2014; Seaton *et al.* 2018), which seems inconsistent with our protein turnover model, the amount of protein on an area basis is maintained or slightly increased due to an increase in LMA (Poorter *et al.* 2019). Also, any anatomical limitation on the capacity of acclimation was not taken into account (Oguchi *et al.* 2003).

Finally, photosynthetic protein degradation rate was assumed identical for both varieties since there is little evidence of differences between species or genotypes (Li *et al.* 2017). Also, its high variability within a functional category and dependency on leaf development, protein abundance (Li *et al.* 2017) and environmental conditions (Peterson *et al.* 1973; Makino *et al.* 1984; Ishihara *et al.* 2015) makes quantification of these effects intricate and implausible using limited data. This assumption advantageously avoids over-parameterizing the model (Eqns 1; see Supporting Information—Eqns S2 and S3), and better differentiates varietal response in protein synthesis. For example, higher $t_d$ was quantified in SC-50 [see Supporting Information—Table S3], suggesting faster $N_p$ turnover during leaf ageing (Table 2) and probably higher nitrogen resorption and reallocation to support high leaf turnover rate (Hikosaka 2005), which is advantageous under field condition with light competition (Hikosaka and Anten 2012).

## SUPPORTING INFORMATION

The following additional information is available in the online version of this article –

## ACKNOWLEDGEMENTS

We thank Ilona Napp, Marlies Lehmann, Adjoa Sekyi-Appiah, Sanzida Akhter Anee and Felliesia Regina Halim for their assistance during the experiments. We also thank Dany Pascal Moualeu-Ngangue and Magnus Adler for their help in programming the GroIMP model. This work was supported by Deutsche Forschungsgemeinschaft (DFG, Project number 403510751).

## CONTRIBUTIONS BY THE AUTHORS

Y.C.P.: Measurements, data curation, data analyses and model simulations. Y.C.P. and T.W.C.: Design of *in silico* experiments, writing of original draft. H.S. and T.W.C.: Conceptualization, funding acquisition, project administration. All authors contributed to manuscript review and editing.

## DATA AVAILABILITY

Data used in this study and models developed are available upon request from the first authors, Yi-Chen Pao, email: pao@gem.uni-hannover.de.

## REFERENCES

Aerts R, Chapin FS III. 1999. The mineral nutrition of wild plants revisited: a re-evaluation of processes and patterns. *Advances in Ecological Research* 30:1–67.

Alqudah AM, Youssef HM, Graner A, Schnurbusch T. 2018. Natural variation and genetic make-up of leaf blade area in spring barley. *Theoretical and Applied Genetics* 131:873–886.

Anten NPR, Schieving F, Werger MJA. 1995. Patterns of light and nitrogen distribution in relation to whole canopy carbon gain in $C_3$ and $C_4$ mono-and dicotyledonous species. *Oecologia* 101:504–513.

Bailey S, Walters RG, Jansson S, Horton P. 2001. Acclimation of *Arabidopsis thaliana* to the light environment: the existence of separate low light and high light responses. *Planta* 213:794–801.

Barnes WC, Epps WM. 1956. Powdery mildew resistance in South Carolina cucumbers. *Plant Disease Reporter* 40:1093.

Brites D, Valladares F. 2005. Implications of opposite phyllotaxis for light interception efficiency of Mediterranean woody plants. *Trees* 19:671–679.

Buckley TN, Cescatti A, Farquhar GD. 2013. What does optimization theory actually predict about crown profiles of photosynthetic capacity when models incorporate greater realism? *Plant, Cell and Environment* 36:1547–1563.

Campbell GS, Norman JM. 1989. The description and measurement of plant canopy structure. In: Russell G, Marshall B, Jarvis PG, eds. *Plant canopies: their growth, form and function*. Cambridge, UK: Cambridge University Press, 1–19.

Cataldo DA, Maroon M, Schrader Le, Youngs VL. 1975. Rapid colorimetric determination of nitrate in plant tissue by nitration of

salicylic acid. *Communications in Soil Science and Plant Analysis* 6:71–80.
Chang T-G, Zhao H, Wang N, Song Q-F, Xiao Y, Qu M, Zhu X-G. 2019. A three-dimensional canopy photosynthesis model in rice with a complete description of the canopy architecture, leaf physiology, and mechanical properties. *Journal of Experimental Botany* 70:2479–2490.
Chen Q, Baldocchi D, Gong P, Dawson T. 2008. Modeling radiation and photosynthesis of a heterogeneous savanna woodland landscape with a hierarchy of model complexities. *Agricultural and Forest Meteorology* 148:1005–1020.
Chen T-W, Cabrera-Bosquet L, Prado SA, Perez RPA, Artzet S, Pradal C, Coupel-Ledru A, Fournier C, Tardieu F. 2019. Genetic and environmental dissection of biomass accumulation in multi-genotype maize canopies. *Journal of Experimental Botany* 70:2523–2534.
Chen T-W, Henke M, de V, Pieter HB, Buck-Sorlin G, Wiechers D, Kahlen K, Stützel H. 2014a. What is the most prominent factor limiting photosynthesis in different layers of a greenhouse cucumber canopy? *Annals of Botany* 114:677–688.
Chen T-W, Nguyen TMN, Kahlen K, Stützel H. 2014b. Quantification of the effects of architectural traits on dry mass production and light interception of tomato canopy under different temperature regimes using a dynamic functional–structural plant model. *Journal of Experimental Botany* 65:6399–6410.
Chen T-W, Nguyen T, Kahlen K, Stützel H. 2015. High temperature and vapor pressure deficit aggravate architectural effects but ameliorate non-architectural effects of salinity on dry mass production of tomato. *Frontiers in Plant Science* 6:887.
Chen T-W, Stützel H, Kahlen K. 2018. High light aggravates functional limitations of cucumber canopy photosynthesis under salinity. *Annals of Botany* 121:797–807.
Criswell AD, Call AD, Wehner TC. 2010. Genetic control of downy mildew resistance in cucumber–a review. *Cucurbit Genetics Cooperative Report* 33:13–16.
Dalin P, Ågren J, Björkman C, Huttunen P, Kärkkäinen K. 2010. Leaf trichome formation and plant resistance to herbivory. In: Schaller A, ed. *Induced plant resistance to herbivory*. Dordrecht, Netherlands: Springer, 89–105.
de Pury DGG, Farquhar GD. 1997. Simple scaling of photosynthesis from leaves to canopies without the errors of big-leaf models. *Plant, Cell & Environment* 20:537–557.
De Vries J, Poelman EH, Anten N, Evers JB. 2018. Elucidating the interaction between light competition and herbivore feeding patterns using functional–structural plant modelling. *Annals of Botany* 121:1019–1031.
DeWitt TJ, Langerhans RB. 2004. Integrated solutions to environmental heterogeneity: theory of multimoment reaction norms. In: DeWitt TJ, Scheiner SM, eds. *Phenotypic plasticity. Functional and conceptual approaches*. New York, NY, USA: Oxford University Press, 98–111.
Drouet J-L, Kiniry JR. 2008. Does spatial arrangement of 3D plants affect light transmission and extinction coefficient within maize crops? *Field Crops Research* 107:62–69.
Duursma RA, Falster DS, Valladares F, Sterck FJ, Pearcy RW, Lusk CH, Sendall KM, Nordenstahl M, Houter NC, Atwell BJ, Kelly N, Kelly JWG, Liberloo M, Tissue DT, Medlyn BE, Ellsworth DS. 2012. Light interception efficiency explained by two simple variables: a test using a diversity of small-to medium-sized woody plants. *New Phytologist* 193:397–408.
Evans JR. 1988. Acclimation by the thylakoid membranes to growth irradiance and the partitioning of nitrogen between soluble and thylakoid proteins. *Functional Plant Biology* 15:93.
Evans JR. 1989. Partitioning of nitrogen between and within leaves grown under different irradiances. *Functional Plant Biology* 16:533–548.
Evans JR. 1993a. Photosynthetic acclimation and nitrogen partitioning within a lucerne canopy. I. Canopy characteristics. *Functional Plant Biology* 20:55–67.
Evans JR. 1993b. Photosynthetic acclimation and nitrogen partitioning within a lucerne canopy. II. Stability through time and comparison with a theoretical optimum. *Functional Plant Biology* 20:69–82.
Evans JR. 2013. Improving photosynthesis. *Plant Physiology* 162:1780–1793.
Evans JR, Clarke VC. 2019. The nitrogen cost of photosynthesis. *Journal of Experimental Botany* 70:7–15.
Evans JR, Poorter H. 2001. Photosynthetic acclimation of plants to growth irradiance: the relative importance of specific leaf area and nitrogen partitioning in maximizing carbon gain. *Plant, Cell & Environment* 24:755–767.
Evans JR, Seemann JR. 1989. The allocation of protein nitrogen in the photosynthetic apparatus: costs, consequences and control. In: Briggs WR, ed. *Photosynthesis*. New York, USA: Alan R. Liss, 183–205.
Falster DS, Westoby M. 2003. Leaf size and angle vary widely across species: what consequences for light interception? *New Phytologist* 158:509–525.
Farquhar GD, von Caemmerer S, Berry JA. 1980. A biochemical model of photosynthetic $CO_2$ assimilation in leaves of $C_3$ species. *Planta* 149:78–90.
Flood PJ, Harbinson J, Aarts MGM. 2011. Natural genetic variation in plant photosynthesis. *Trends in Plant Science* 16:327–335.
Hikosaka K. 2004. Interspecific difference in the photosynthesis–nitrogen relationship: patterns, physiological causes, and ecological importance. *Journal of Plant Research* 117:481–494.
Hikosaka K. 2005. Leaf canopy as a dynamic system: ecophysiology and optimality in leaf turnover. *Annals of Botany* 95:521–533.
Hikosaka K. 2005. Nitrogen partitioning in the photosynthetic apparatus of *Plantago asiatica* leaves grown under different temperature and light conditions: similarities and differences between temperature and light acclimation. *Plant and Cell Physiology* 46:1283–1290.
Hikosaka K. 2010. Mechanisms underlying interspecific variation in photosynthetic capacity across wild plant species. *Plant Biotechnology* 27:223–229.
Hikosaka K. 2014. Optimal nitrogen distribution within a leaf canopy under direct and diffuse light. *Plant, Cell & Environment* 37:2077–2085.
Hikosaka K. 2016. Optimality of nitrogen distribution among leaves in plant canopies. *Journal of Plant Research* 129:299–311.
Hikosaka K, Anten NPR. 2012. An evolutionary game of leaf dynamics and its consequences for canopy structure. *Functional Ecology* 26:1024–1032.
Hikosaka K, Anten NPR, Borjigidai A, Kamiyama C, Sakai H, Hasegawa T, Oikawa S, Iio A, Watanabe M, Koike T, Nishina K, Ito A. 2016. A meta-analysis of leaf nitrogen distribution within plant canopies. *Annals of Botany* 118:239–247.
Hikosaka K, Hirose T. 1997. Leaf angle as a strategy for light competition: optimal and evolutionarily stable light-extinction coefficient within a leaf canopy. *Écoscience* 4:501–507.
Hikosaka K, Terashima I. 1996. Nitrogen partitioning among photosynthetic components and its consequence in sun and shade plants. *Functional Ecology* 10:335–343.
Honda H, Fisher JB. 1978. Tree branch angle: maximizing effective leaf area. *Science* 199:888–890.
Ishihara H, Obata T, Sulpice R, Fernie AR, Stitt M. 2015. Quantifying protein synthesis and degradation in Arabidopsis by dynamic $^{13}CO_2$ labeling and analysis of enrichment in individual amino acids in their free pools and in protein. *Plant Physiology* 168:74–93.
Ishimaru K, Kobayashi N, Ono K, Yano M, Ohsugi R. 2001. Are contents of Rubisco, soluble protein and nitrogen in flag leaves of rice controlled by the same genetics? *Journal of Experimental Botany* 52:1827–1833.
Kahlen K, Stützel H. 2011. Modelling photo-modulated internode elongation in growing glasshouse cucumber canopies. *New Phytologist* 190:697–708.
Kahlen K, Wiechers D, Stützel H. 2008. Modelling leaf phototropism in a cucumber canopy. *Functional Plant Biology* 35:876–884.
Kimball BA, Bellamy LA. 1986. Generation of diurnal solar radiation, temperature, and humidity patterns. *Energy in Agriculture* 5:185–197.
Kniemeyer O. 2008. *Design and implementation of a graph grammar based language for functional-structural plant modelling*. PhD Thesis, Brandenburg University of Technology, Cottbus-Senftenberg, Germany.

Li L, Nelson CJ, Trösch J, Castleden I, Huang S, Millar AH. 2017. Protein degradation rate in *Arabidopsis thaliana* leaf growth and development. *The Plant Cell* 29:207–228.

Lichtenthaler H. 1987. Chlorophylls and carotenoids: pigments of photosynthetic biomembranes. *Methods in Enzymology* 148:350–382.

Long SP, Ainsworth EA, Rogers A, Ort DR. 2004. Rising atmospheric carbon dioxide: plants FACE the future. *Annual Review of Plant Biology* 55:591–628.

Maddonni GA, Chelle M, Drouet J-L, Andrieu B. 2001a. Light interception of contrasting azimuth canopies under square and rectangular plant spatial distributions: simulations and crop measurements. *Field Crops Research* 70:1–13.

Maddonni GA, Otegui ME, Cirilo AG. 2001b. Plant population density, row spacing and hybrid effects on maize canopy architecture and light attenuation. *Field Crops Research* 71:183–193.

Makino A, Mae T, Ohira K. 1984. Relation between nitrogen and ribulose-1,5-bisphosphate carboxylase in rice leaves from emergence through senescence. *Plant and Cell Physiology* 25:429–437.

Mantilla-Perez MB, Salas Fernandez MG. 2017. Differential manipulation of leaf angle throughout the canopy: current status and prospects. *Journal of Experimental Botany* 68:5699–5717.

Mettler T, Mühlhaus T, Hemme D, Schöttler M-A, Rupprecht J, Idoine A, Veyel D, Pal SK, Yaneva-Roder L, Winck FV, Sommer F, Vosloh D, Seiwert B, Erban A, Burgos A, Arvidsson S, Schönfelder S, Arnold A, Günther M, Krause U, Lohse M, Kopka J, Nikoloski Z, Mueller-Roeber B, Willmitzer L, Bock R, Schroda M, Stitt M. 2014. Systems analysis of the response of photosynthesis, metabolism, and growth to an increase in irradiance in the photosynthetic model organism *Chlamydomonas reinhardtii*. *The Plant Cell* 26:2310–2350.

Miller MAE, O'Cualain R, Selley J, Knight D, Karim MF, Hubbard SJ, Johnson GN. 2017. Dynamic acclimation to high light in *Arabidopsis thaliana* involves widespread reengineering of the leaf proteome. *Frontiers in Plant Science* 8:1239.

Monsi M, Saeki T. 2005. On the factor light in plant communities and its importance for matter production. *Annals of Botany* 95:549–567.

Muller B, Martre P. 2019. Plant and crop simulation models: powerful tools to link physiology, genetics, and phenomics. *Journal of Experimental Botany* 70:2339–2344.

Muller O, Hikosaka K, Hirose T. 2005. Seasonal changes in light and temperature affect the balance between light harvesting and light utilisation components of photosynthesis in an evergreen understory shrub. *Oecologia* 143:501–508.

Murata N, Takahashi S, Nishiyama Y, Allakhverdiev SI. 2007. Photoinhibition of photosystem II under environmental stress. *Biochimica et Biophysica Acta* 1767:414–421.

Murchie EH, Niyogi KK. 2011. Manipulation of photoprotection to improve plant photosynthesis. *Plant Physiology* 155:86–92.

Nelson DW, Sommers LE. 1980. Total nitrogen analysis of soil and plant tissues. *Journal of the Association of Official Analytical Chemists* 63:770–778.

Niinemets U, Keenan TF, Hallik L. 2015. A worldwide analysis of within-canopy variations in leaf structural, chemical and physiological traits across plant functional types. *New Phytologist* 205:973–993.

Niinemets U, Portsmuth A, Tena D, Tobias M, Matesanz S, Valladares F. 2007. Do we underestimate the importance of leaf size in plant economics? Disproportional scaling of support costs within the spectrum of leaf physiognomy. *Annals of Botany* 100:283–303.

Niklas KJ. 2013. Biophysical and size-dependent perspectives on plant evolution. *Journal of Experimental Botany* 64:4817–4827.

Niklas KJ, Hammond ST. 2013. Biophysical effects on plant competition and coexistence. *Functional Ecology* 27:854–864.

Oguchi R, Hikosaka K, Hirose T. 2003. Does the photosynthetic light-acclimation need change in leaf anatomy? *Plant, Cell and Environment* 26:505–512.

Okabe T. 2015. Biophysical optimality of the golden angle in phyllotaxis. *Scientific Reports* 5:1–7.

Onoda Y, Hikosaka K, Hirose T. 2004. Allocation of nitrogen to cell walls decreases photosynthetic nitrogen-use efficiency. *Functional Ecology* 18:419–425.

Osada N, Yasumura Y, Ishida A. 2014. Leaf nitrogen distribution in relation to crown architecture in the tall canopy species, *Fagus crenata*. *Oecologia* 175:1093–1106.

Pao Y-C, Chen T-W, Moualeu-Ngangue DP, Stützel H. 2019a. Environmental triggers for photosynthetic protein turnover determine the optimal nitrogen distribution and partitioning in the canopy. *Journal of Experimental Botany* 70:2419–2434.

Pao Y-C, Chen T-W, Moualeu-Ngangue DP, Stützel H. 2020. Experiments for *in silico* evaluation of optimality of photosynthetic nitrogen distribution and partitioning in the canopy: an example using greenhouse cucumber plants. *Bio-Protocol* 10:e3556.

Pao Y-C, Kahlen K, Chen T-W, Wiechers D, Stützel H. 2021. How does structure matter? Comparison of canopy photosynthesis using one- and three-dimensional light models: a case study using greenhouse cucumber canopies. *in silico Plants* 3:diab031.

Pao Y-C, Stützel H, Chen T-W. 2019b. A mechanistic view of the reduction in photosynthetic protein abundance under diurnal light fluctuation. *Journal of Experimental Botany* 70:3705–3708.

Papadopoulos AP, Hao X. 2000. Effects of day and night air temperature on growth, productivity and energy use of long English cucumber. *Canadian Journal of Plant Science* 80:143–150.

Pearcy RW, Valladares F, Wright SJ, Paulis EL de. 2004. A functional analysis of the crown architecture of tropical forest Psychotria species: do species vary in light capture efficiency and consequently in carbon gain and growth? *Oecologia* 139:163–177.

Perez RPA, Dauzat J, Pallas B, Lamour J, Verley P, Caliman J-P, Costes E, Faivre R. 2018. Designing oil palm architectural ideotypes for optimal light interception and carbon assimilation through a sensitivity analysis of leaf traits. *Annals of Botany* 121:909–926.

Perez RPA, Fournier C, Cabrera-Bosquet L, Artzet S, Pradal C, Brichet N, Chen T-W, Chapuis R, Welcker C, Tardieu F. 2019. Changes in the vertical distribution of leaf area enhanced light interception efficiency in maize over generations of selection. *Plant, Cell & Environment* 42:2105–2119.

Peterson LW, Kleinkopf GE, Huffaker RC. 1973. Evidence for lack of turnover of ribulose 1, 5-diphosphate carboxylase in barley leaves. *Plant Physiology* 51:1042–1045.

Pons TL, Anten NPR. 2004. Is plasticity in partitioning of photosynthetic resources between and within leaves important for whole-plant carbon gain in canopies? *Functional Ecology* 18:802–811.

Poorter H, Niinemets U, Ntagkas N, Siebenkäs A, Mäenpää M, Matsubara S, Pons T. 2019. A meta-analysis of plant responses to light intensity for 70 traits ranging from molecules to whole plant performance. *New Phytologist* 223:1073–1105.

Poorter H, Niinemets U, Poorter L, Wright IJ, Villar R. 2009. Causes and consequences of variation in leaf mass per area (LMA): a meta-analysis. *The New Phytologist* 182:565–588.

R Core Team. 2019. *R. A language and environment for statistical computing*. Vienna, Austria: R Core Team.

Sadras VO, Richards RA. 2014. Improvement of crop yield in dry environments: benchmarks, levels of organisation and the role of nitrogen. *Journal of Experimental Botany* 65:1981–1995.

Savvides A, Dieleman JA, van Ieperen W, Marcelis LFM. 2016. A unique approach to demonstrating that apical bud temperature specifically determines leaf initiation rate in the dicot *Cucumis sativus*. *Planta* 243:1071–1079.

Schieving F, Poorter H. 1999. Carbon gain in a multispecies canopy: the role of specific leaf area and photosynthetic nitrogen-use efficiency in the tragedy of the commons. *New Phytologist* 143:201–211.

Seaton DD, Graf A, Baerenfaller K, Stitt M, Millar AJ, Gruissem W. 2018. Photoperiodic control of the Arabidopsis proteome reveals a translational coincidence mechanism. *Molecular Systems Biology* 14:e7962.

Shetty NV, Wehner TC. 2002. Screening the cucumber germplasm collection for fruit yield and quality. *Crop Science* 42:2174–2183.

Song Q, Wang Y, Qu M, Ort DR, Zhu X-G. 2017. The impact of modifying photosystem antenna size on canopy photosynthetic efficiency. *Plant, Cell & Environment* 40:2946–2957.

Song Q, Zhang G, Zhu X-G. 2013. Optimal crop canopy architecture to maximise canopy photosynthetic $CO_2$ uptake under elevated $CO_2$–a theoretical study using a mechanistic model of canopy photosynthesis. *Functional Plant Biology* 40:108–124.

Strauss S, Lempe J, Prusinkiewicz P, Tsiantis M, Smith RS. 2020. Phyllotaxis: is the golden angle optimal for light capture? *The New Phytologist* 225:499–510.

Strauss-Debenedetti S, Bazzaz FA. 1991. Plasticity and acclimation to light in tropical Moraceae of different sucessional positions. *Oecologia* 87:377–387.

Tahiri AZ, Anyoji H, Yasuda H. 2006. Fixed and variable light extinction coefficients for estimating plant transpiration and soil evaporation under irrigated maize. *Agricultural Water Management* 84:186–192.

Tang L, Yin D, Chen C, Yu D, Han W. 2019. Optimal design of plant canopy based on light interception: A case study with loquat. *Frontiers in Plant Science* 10:364.

Taylor SH, Orr DJ, Carmo-Silva E, Long SP. 2020. During photosynthetic induction, biochemical and stomatal limitations differ between *Brassica* crops. *Plant, Cell & Environment* 43:2623–2636. doi:10.1111/pce.13862.

Terashima I, Evans JR. 1988. Effects of light and nitrogen nutrition on the organization of the photosynthetic apparatus in spinach. *Plant and Cell Physiology* 29:143–155.

Tian D, Traw MB, Chen JQ, Kreitman M, Bergelson J. 2003. Fitness costs of R-gene-mediated resistance in *Arabidopsis thaliana*. *Nature* 423:74–77.

Todesco M, Balasubramanian S, Hu TT, Traw MB, Horton M, Epple P, Kuhns C, Sureshkumar S, Schwartz C, Lanz C, Laitinen RAE, Huang Y, Chory J, Lipka V, Borevitz JO, Dangl JL, Bergelson J, Nordborg M, Weigel D. 2010. Natural allelic variation underlying a major fitness trade-off in *Arabidopsis thaliana*. *Nature* 465:632–636.

Trouwborst G, Hogewoning SW, Harbinson J, van Ieperen W. 2011. Photosynthetic acclimation in relation to nitrogen allocation in cucumber leaves in response to changes in irradiance. *Physiologia Plantarum* 142:157–169.

Trouwborst G, Oosterkamp J, Hogewoning SW, Harbinson J, van Ieperen W. 2010. The responses of light interception, photosynthesis and fruit yield of cucumber to LED-lighting within the canopy. *Physiologia Plantarum* 138:289–300.

Truong SK, McCormick RF, Rooney WL, Mullet JE. 2015. Harnessing genetic variation in leaf angle to increase productivity of *Sorghum bicolor*. *Genetics* 201:1229–1238.

Verkroost AWM, Wassen MJ. 2005. A simple model for nitrogen-limited plant growth and nitrogen allocation. *Annals of Botany* 96:871–876.

Werger MJA, Hirose T. 1991. Leaf nitrogen distribution and whole canopy photosynthetic carbon gain in herbaceous stands. *Vegetatio* 97:11–20.

Whitman T, Aarssen LW. 2010. The leaf size/number trade-off in herbaceous angiosperms. *Journal of Plant Ecology* 3:49–58.

Wright IJ, Reich PB, Westoby M, Ackerly DD, Baruch Z, Bongers F, Cavender-Bares J, Chapin T, Cornelissen JHC, Diemer M, Flexas J, Garnier E, Groom PK, Gulias J, Hikosaka K, Lamont BB, Lee T, Lee W, Lusk C, Midgley JJ, Navas M-L, Niinemets U, Oleksyn J, Osada N, Poorter H, Poot P, Prior L, Pyankov VI, Roumet C, Thomas SC, Tjoelker MG, Veneklaas EJ, Villar R. 2004. The worldwide leaf economics spectrum. *Nature* 428:821–827.

Yin X, Schapendonk AH, Struik PC. 2019. Exploring the optimum nitrogen partitioning to predict the acclimation of $C_3$ leaf photosynthesis to varying growth conditions. *Journal of Experimental Botany* 70:2435–2447.

Zhang H, Li S, Yang L, Cai G, Chen H, Gao D, Lin T, Cui Q, Wang D, Li Z, Cai R, Bai S, Lucas WJ, Huang S, Zhang Z, Sun J. 2021. Gain-of-function of the 1-aminocyclopropane-1-carboxylate synthase gene *ACS1G* induces female flower development in cucumber gynoecy. *The Plant Cell* 33:306–321.

Zhang L, Hu Z, Fan J, Zhou D, Tang F. 2014. A meta-analysis of the canopy light extinction coefficient in terrestrial ecosystems. *Frontiers of Earth Science* 8:599–609.

Zhu X-G, Long SP, Ort DR. 2010. Improving photosynthetic efficiency for greater yield. *Annual Review of Plant Biology* 61:235–261.